Received: 5 August 2024 | Revised: 18 November 2024 | Accepted: 17 December 2024

DOI: 10.1002/jev2.70035

RESEARCH ARTICLE

# Direct delivery of immune modulators to tumour-infiltrating lymphocytes using engineered extracellular vesicles

**Xiabing Lyu**[1,2] | **Tomoyoshi Yamano**[1,2] | **Kanto Nagamori**[2] | **Shota Imai**[2] | **Toan Van Le**[2] | **Dilireba Bolidong**[1] | **Makie Ueda**[2] | **Shota Warashina**[3,4] | **Hidefumi Mukai**[3,4] | **Seigo Hayashi**[5] | **Kazutaka Matoba**[5] | **Taito Nishino**[5] | **Rikinari Hanayama**[1,2]

[1]WPI Nano Life Science Institute (NanoLSI), Kanazawa University, Kanazawa, Japan

[2]Department of Immunology, Graduate School of Medicine, Kanazawa University, Kanazawa, Japan

[3]Laboratory for Molecular Delivery and Imaging Technology, RIKEN Center for Biosystems Dynamics Research, Kobe, Japan

[4]Department of Pharmaceutical Informatics, Graduate School of Biomedical Sciences, Nagasaki University, Nagasaki, Japan

[5]Biological Research Laboratories, Nissan Chemical Corporation, Saitama, Japan

**Correspondence**
Tomoyoshi Yamano and Rikinari Hanayama, WPI Nano Life Science Institute (NanoLSI), Kanazawa University, Kanazawa, Japan. Email: tomoyoshi.yamano@med.kanazawa-u.ac.jp and rikinari-hanayama@umin.ac.jp

**Funding information**
Japan Agency for Medical Research and Development, Grant/Award Numbers: 22am0401019h0004, JP23ak0101178; Japan Science and Technology Corporation, Grant/Award Numbers: JPMJCR18H4, JPMJFR2115, JPMJPR19HA

**Abstract**

Extracellular vesicles (EVs) are important mediators of cell–cell communication, including immune regulation. Despite the recent development of several EV-based cancer immunotherapies, their clinical efficacy remains limited. Here, we created antigen-presenting EVs to express peptide-major histocompatibility complex (pMHC) class I, costimulatory molecule and IL-2. This enabled the selective delivery of multiple immune modulators to antigen-specific $CD8^+$ T cells, promoting their expansion in vivo without severe adverse effects. Notably, antigen-presenting EVs accumulated in the tumour microenvironment, increasing IFN-$\gamma^+$ $CD8^+$ T cell and decreasing exhausted $CD8^+$ T cell numbers, suggesting that antigen-presenting EVs transformed the 'cold' tumour microenvironment into a 'hot' one. Combination therapy with antigen-presenting EVs and anti-PD-1 demonstrated enhanced anticancer immunity against established tumours. We successfully engineered humanized antigen-presenting EVs, which selectively stimulated tumour antigen-specific $CD8^+$ T cells. In conclusion, engineering EVs to co-express multiple immunomodulators represents a promising method for cancer immunotherapy.

**KEYWORDS**
antigen presentation, cancer immunotherapy, drug delivery, extracellular vesicle, targeted cytokine delivery

## 1 | INTRODUCTION

Cancer remains a leading cause of mortality worldwide, despite advancements in traditional treatment modalities such as chemo-, radiation and immunotherapy. These approaches often lack specificity, resulting in off-target damage to healthy tissues and severe side effects. Furthermore, suboptimal drug bioavailability within tumour tissues often requires the administration of higher doses to achieve therapeutic effects. These increased doses can exacerbate toxicity in normal cells and potentially promote the emergence of multi-drug resistance in cells exposed to suboptimal drug concentrations (Holohan et al., 2013). Therefore, there is an urgent need for innovative therapeutic strategies that can target tumours with greater selectivity and efficacy.

Nanoparticles have emerged as a promising platform for drug delivery in cancer therapy. These nanoscale carriers exhibit unique physicochemical properties that enable the efficient delivery of therapeutic agents, including drugs, DNA, RNA and

Xiabing Lyu and Tomoyoshi Yamano contributed equally to this work.

proteins, directly to cancer cells (Blanco et al., 2015). Among them, extracellular vesicles (EVs), including exosomes, are promising nanovesicles for use in clinical settings owing to their biocompatibility, low immunogenicity and high drug delivery efficiency (Cheng & Hill, 2022). EVs contain various proteins, lipids and RNAs that induce functional and physiological changes in target cells (van Niel et al., 2018). EVs released by cancer or antigen-presenting cells reportedly modulate immune responses (Robbins & Morelli, 2014). For example, cancer-derived EVs express PD-L1, a ligand of the inhibitory receptor PD-1 on T cells, which hampers the anticancer immune response (Chen et al., 2018; Poggio et al., 2019). In contrast, mature dendritic cell (DC)-derived exosomes express peptide-major histocompatibility complex (pMHC), which can directly or indirectly stimulate T cells (Pitt et al., 2016). The stimulatory properties of DC-derived exosomes have shown promising results in cancer immunotherapy (Li et al., 2023; Lu et al., 2017; Zitvogel et al., 1998). However, few clinical studies have demonstrated the therapeutic effect of EVs against cancer, possibly because of the limitations of costimulatory molecules and cytokines (Besse et al., 2016).

Cytokines play a pivotal role in regulating immune homeostasis, and their quantities are crucial in clinical immunotherapy (Berraondo et al., 2019; Briukhovetska et al., 2021). Cytokines are highly effective locally but have severe adverse effects when used systemically. For example, IL-2 improved T cell immunity in patients with metastatic melanoma and renal cell carcinoma (Atkins et al., 1999; Rosenberg et al., 1993). However, high IL-2 doses activated endothelial cells, which express high-affinity IL-2R$\alpha$, leading to vascular leak syndrome (Yang et al., 2003). In addition, IL-2 increased the number of regulatory T cells (Tregs), weakening the immune response to cancer (Ahmadzadeh & Rosenberg, 2006). Several strategies have been developed to overcome these challenges, including the engineering of IL-2 variants that selectively stimulate memory $CD8^+$ T and natural killer (NK) cells. These IL-2 variants bind preferentially to IL-2R$\beta$, thereby reducing the undesirable expansion of Tregs and associated adverse events (Boyman et al., 2006; Levin et al., 2012; Ren et al., 2022). Another approach involves a fusion protein that combines IL-2 with the orthopoxvirus major histocompatibility complex (MHC) class I-like protein (OMCP), a recognized ligand of NKG2D, directing IL-2 specifically to NKG2D-positive cells (Ghasemi et al., 2016). Despite these advances, IL-2 variants and IL-2-OMCP fusion proteins primarily act on polyclonal $CD8^+$ T cells, many of which lack antigen specificity against tumours. Thus, the targeted delivery of IL-2 to antigen-specific $CD8^+$ T cells remain limited.

To address these challenges and harness the potential of EVs in actively targeting immune modulators, we engineered antigen-presenting EVs (AP-EVs) and explored their potential in enhancing specific T cell responses. By incorporating pMHC, costimulatory molecules, and IL-2 into EVs, we aimed to selectively deliver these immune modulators to tumour-specific T cells, thereby promoting a robust and targeted immune response against cancer.

## 2 | MATERIALS AND METHODS

### 2.1 | Resource availability

#### 2.1.1 | Lead contact

Further information and requests for resources should be directed to the lead contact, Dr. Tomoyoshi Yamano.

#### 2.1.2 | Materials availability

Plasmids generated in this study are available from the corresponding author upon reasonable request.

### 2.2 | Experimental design

This study aimed to engineer EVs with enhanced functionality for cancer immunotherapy. To extensively stimulate antigen-specific $CD8^+$ T cells, we utilized EV engineering technology to concurrently express multiple immune modulators in AP-EVs. AP-EVs were evaluated using nanoparticle tracking analysis, confocal microscopy, nanoFCM, immunoblotting, electron microscope and flow cytometry to analyse their size, concentration and surface proteins. PET imaging was used to assess the in vivo distribution of AP-EVs. Mice were randomly assigned to different experimental groups for in vivo studies. One mouse in the combination therapy group unexpectedly died during tumour measurement, and its data were excluded from subsequent analyses.

### 2.3 | Cell lines

Human embryonic kidney (HEK293 or HEK293T), retroviral packaging (PLAT-A), and lenti-X cells (Takara) were cultured in Dulbecco's modified Eagle's medium (Thermo Fisher Scientific) supplemented with 10% heat-inactivated foetal calf serum (FCS; Thermo Fisher Scientific), 100 U/mL penicillin, and 100 U/mL streptomycin (FUJIFILM Wako). Cells of an

ovalbumin-expressing murine lymphoma cell line, an EL4 derivative (E.G7; ATCC, CRL-2113), and murine lymphocytes were cultured in RPMI (Nacalai Tesque) supplemented with 10% FCS, 1× non-essential amino acid (Nacalai Tesque), 1 nmol/L sodium pyruvate (Nacalai Tesque), 100 U/mL penicillin, 100 U/mL streptomycin (FUJIFILM Wako), and 0.05 μM 2-mercaptoethanol (Thermo Fisher Scientific). All the cells were cultured at 37°C in a humidified atmosphere containing 5% $CO_2$. To prepare EV-free FCS, FCS was mixed with 50% PEG-10,000 (Merck) at a 5:1 ratio and rotated at 4°C for 3 h, PEG was removed by centrifugation at 2000 × *g* for 20 min, and the supernatant was filtered through a 0.22-μm strainer and collected. The AP-EV-producing cell line was cultured in advanced Dulbecco's modified Eagle's medium supplemented with 2% EV-depleted FCS, 1 nmol/L sodium pyruvate, 100 U/mL penicillin and 100 U/mL streptomycin.

## 2.4 | Mice

C57BL/6 was purchased from Japan SLC and Jackson Laboratory. OT-I TCR transgenic mice (CD45.1) were established as previously described. (Hogquist et al., 1994) All mice were housed in a specific pathogen-free facility.

## 2.5 | Preparation and purification of AP-EVs

HEK293 cells stably expressing OVA peptide-single-chain trimer-CD81-IL2 and CD80-CD9 fusion proteins were generated using a retroviral system. Virus titres were measured by qPCR using the Retrovirus Titer Set for Real-Time PCR (Takara, 6166). The MOI of the OVA-scCD81IL2 virus was 6340, and the MOI of the CD80-CD9 virus was 2031 for infection. HEK293 cells with high expression levels of OVA-scCD81IL2 and CD80-CD9 fusion proteins were sorted using the BD Melody cell sorter, and a single colony with the highest expression was established by limiting dilution. This single colony of AP-EV stable cells was used for further EV production.

For AP-EV purification, the cell culture supernatant was first centrifuged at 300 × *g* for 5 min to remove cell debris and then re-centrifuged at 1200 × *g* for 20 min to remove cell debris and apoptotic bodies. The supernatant was again centrifuged at 10,000 × *g* for 30 min to remove apoptotic bodies and large EVs. AP-EVs were isolated from the supernatant through centrifugation at 100,000 × *g* for 4 h, the pellet was washed with phosphate-buffered saline (PBS), and the AP-EV concentration was determined using a bicinchoninic acid (BCA) assay (Thermo Fisher Scientific).

## 2.6 | Nanoparticle tracking analysis

The number and characteristics of AP-EVs were determined using a NanoSight LM10 (Malvern Panalytical, Malvern, UK). Briefly, 600 μL of diluted AP-EV solution was placed on a sample stage, and EP-EV motion was captured at a camera level of 15 for 30 s. Three distinct fields were recorded, and data were analysed using NanoSight NTA version 3.1 software (Malvern Panalytical) with a detection threshold of three.

## 2.7 | Confocal microscopy

EVs were isolated from CD81-RFP and CD9-GFP co-transfected HEK293T cells using ultracentrifugation, as described in 'Preparation and purification of AP-EVs'. The EV suspension was passed through a 0.22-μm filter and diluted to $2 \times 10^8$ particles/30 μL PBS. A 30-μL suspension was applied onto a glass slide and covered with a cover slip. EVs were visualized through a 100× oil immersion lens using confocal fluorescence microscopy (Nikon A1R). The colocalization of GFP and RFP was imaged and quantified using Imaris software (Oxford Instruments, Oxfordshire, UK).

## 2.8 | Antibodies

Antibody staining was performed according to standard procedures. Monoclonal antibodies for surface staining, including antibodies against mCD3 (clone: 17A2), mCD4 (clone: GK1.5), mCD8α (clone: 53–6.7), mCD19 (clone: 6D5), mCD25 (clone: PC61), mNK1.1 (clone: S17016D), mTCR-Vβ5.1,5.2 (clone: MR9-4), mCD45 (clone: 30-F11), mCD45.1 (clone: A20), mCD45.2 (clone: 104), mCD44 (clone: IM7), mCD62L (clone: MEL-14), mH-$2K^b$ bound to SIINFEKL-APC (clone: 25-D1.16), mCD80 (clone: 16-10A1), mIL-2 (clone: JES6-5H4), mPD1 (clone: EH12.2H7), hCD8 (clone: SK1), hCD3 (clone: OKT3), hCD69 (clone: FN50) and hCD54 (clone: HA58) were purchased from BioLegend. An antibody against human TCRβ13.1 (clone: H131) was purchased from Invitrogen. Intracellular staining was performed using antibodies against mIFN-γ (clone: XMG1.2), mGranzyme B (clone: MF-14), mFoxp3 (clone: 53–6.7), hIFN-γ (clone: 4S.B3), hGranzyme B (clone: QA16A02), and Nur77 (clone: 12.16). OVA-specific $CD8^+$ T cells were quantified using the H-$2K^b$/OVA (257–264) tetramer (Tetramer Shop) according to the manufacturer' s instructions.

## 2.9 | Flow cytometric analysis of EVs

The EV-surface levels of OVAp-MHCI, CD80 and IL-2 were assessed using a PS Capture Exosome flow cytometry kit (FUJIFILM Wako) according to the manufacturer's instructions. Briefly, the supernatant obtained after centrifugation at 10,000 × *g* for 30 min was purified and incubated with EV capture beads for 1 h. The EV-bound beads were stained with APC conjugated anti-mouse H-2K$^{b}$ bound to SIINFEKL antibody (clone: 25-D1.16), PE-conjugated anti CD80 antibody (clone: 16-10A1), and APC conjugated anti-mouse IL-2 antibody (clone: JES6-5H4). All antibodies were diluted 100 times. The beads were incubated at room temperature for 1 h, vortexed every 20 min, washed, and analysed using a CytoFLEX flow cytometer (Beckman Coulter); the data were processed using FlowJo software version 10.4.1 (Ashland, OR, USA).

## 2.10 | Single EV analysis using NanoFCM

Single EV analysis was performed as previously described. (Kobayashi et al., 2024) Briefly, EVs ($4.0 \times 10^{9}$ particles) were purified by ultracentrifugation, then stained with fluorescence-conjugated antibodies at a 1:10 dilution in 40 μL of immobilizing buffer from the MagCapture Exosome Isolation Kit PS Ver.2 (FUJIFILM Wako Pure Chemical) at room temperature for 2 h. After staining, 960 μL of immobilizing buffer with a binding enhancer was added to the stained EVs. Antibody-conjugated EVs were further purified by incubating with Tim4 beads, which were prepared by mixing 0.06 mg of streptavidin magnetic beads with 0.1 μg of TIM4-biotin. EVs were eluted from TIM4-beads by incubating the beads for 10 min in 40 μL of elution buffer in two sequential elution steps. The EVs were analysed using a Flow Nanoanalyzer (NanoFCM, Xiamen, China) equipped with two lasers (488 and 638 nm) and three band-pass filters (488/10, 525/40 and 670/40). All measurements were performed according to the manufacturer' s protocol. Briefly, Milli-Q water was filtered through a Millex-GS 0.22 μm MCE membrane (Merck) three times for use of the sheath flow of EV flow cytometry. Silica nanoparticle cocktail (68–155 nm, NanoFCM) and polystyrene 250 nm beads (QC Beads, NanoFCM) were used as the size and particle concentration references, respectively. PBS (–) was measured to determine a threshold for the SS-H channel, which was set to 'mean + 3 × SD' of SS-H in PBS (–). EVs were diluted with PBS (–) at a concentration of $1.0 \times 10^{8-9}$ EVs/mL to run EVs at a flow rate of 50–200 events per second and more than 3000 events were recorded during 60 s of measurement. All samples were run under identical pressure (1 kPa), and the signals of SS, FITC and APC were recorded. The data were processed using FlowJo software version 10.4.1 (Ashland, OR, USA).

## 2.11 | AFM analysis

EVs were immobilized on a poly-L-lysine-modified mica substrate. A Bruker BioScope Resolve AFM system operated in the peak force tapping mode was used for imaging and nanomechanical analysis as previously described. (Yurtsever et al., 2021) AFM images were captured using 240 AC-NG cantilevers with the spring constant set using the thermal tuning method. The peak force tapping amplitude, frequency and setpoint were set to 20–50 nm, 1 kHz, and 0.5–2 nN, respectively. Young' s modulus was measured using quantitative nanomechanical mapping and the Sneddon contact mechanical model from a typical 256 × 256-pixel scan. AFM image rendering and nanomechanical data processing were performed using NanoScope Analysis software version 1.9.

## 2.12 | Electron microscopy analysis

EV samples were purified using the MagCapture Exosome Isolation Kit PS Ver.2, following the manufacturer's instructions. EVs samples ($5 \times 10^{10}$ particles/mL) were then sent to Hanaichi UltraStructure Research Institute (Japan) for electron microscopy (EM) imaging. The samples were negatively stained by placing a droplet of the sample on a carbon-film grid for 10 s, blotting off excess liquid, and adding a drop of 2% uranyl acetate staining solution for 10 s. The grid was then blotted and dried at room temperature. The samples were observed using a JEOL JEM-1400Flash electron microscope at 100kV.

## 2.13 | Western blot analysis

For cell lysate samples, 293 cells were lysed using RIPA buffer (50 mmol/L Tris-HCl, pH 8.0, 150 mM sodium chloride, 1% NP-40, 0.5% sodium deoxycholate, 0.1% sodium dodecyl sulphate and 2 mM EDTA) containing 1 mM PMSF protease inhibitor. The lysates were centrifuged at 12,000 rpm at 4°C for 10 min. Protein concentration was quantified using a BCA Protein Assay Kit (Thermo Fisher Scientific). For EV samples, EVs were isolated from the supernatants of 293 cells and AP-EVs stable cell lines via ultracentrifugation. A total of 21 μg of cell lysate protein and $4.3 \times 10^{7}$ particles were analysed using the Simple Western Wes Instrument (Bio-Techne, ProteinSimple). Western blot analysis was performed using the following primary antibodies: anti-human $\beta$-actin (Sigma-Aldrich, clone: AC-15; 1:100), anti-human GAPDH (MBL, clone: 3H12; 1:100), anti-human TSG101

(GeneTex, clone: GTX118736; 1:100), anti-human CD81 (BioLegend, clone: 5A6; 1:100), anti-mouse CD9 (Thermo Fisher, clone: EM-04;1:100), and anti-mouse IL-2 (BioLegend, clone: JES6-1A12; 1:100). The secondary antibodies used were HRP Goat anti-mouse IgG (BioLegend, clone: Poly4053; 1:300), HRP Goat anti-rat IgG (BioLegend, clone: Poly4054; 1:300), and HRP Donkey anti-rabbit IgG (BioLegend, clone: Poly4064; 1:300).

## 2.14 | IL-2 bioassay

CTLL-2 cells were seeded in 96-well plates at $8 \times 10^4$ cells/well, and serial AP-EV dilutions were added to each well. Cell viability was measured after 3 days of culturing using a WST-I colorimetric assay (Nacalai Tesque).

## 2.15 | In vitro T cell proliferation assay

LN T cells from OT-I transgenic mice were labelled with 1 μM CTV (Thermo Fisher Scientific) at 37°C for 3 min. In total, $2 \times 10^5$ CTV-labelled OT-I T cells were co-cultured with AP-EVs or control EVs at concentrations of 3, 1, 0.3 and 0.1 μg/mL or anti-mouse CD3/CD28 beads (Thermo Fisher Scientific) for 3 days. OT-I T cell proliferation was evaluated using flow cytometry. To test the cytotoxic ability of activated OT-I T cells, OT-I T cells were cocultured with AP-EV for 3 days in vitro. After coculture, the cells were fixed using the True-Nuclear Transcription Factor Buffer Set (BioLegend) following cell surface staining. The production of granzyme B and IFN-$\gamma$ was measured by intracellular staining using antibodies against mouse IFN-$\gamma$ (Biolegend, clone: XMG1.2; 1:50) and mouse granzyme B (Biolegend, clone: MF-14; 1:50).

## 2.16 | Adoptive T cell transfer

LN T cells from OT-I (CD45.1) and C57BL/6 mice (CD45.2) were mixed at a 1:1 ratio and labelled with CTV. In total, $2 \times 10^6$ T cells were intravenously injected into CD45.1/CD45.2 recipient mice. After 1 day, the recipient mice were treated with either 50 μg AP-EVs, 50 μg control EVs or IL-2/IL-2 mAb, which comprised 1.5 μg mouse recombinant IL-2 (BioLegend) and 50 μg anti-IL-2 monoclonal antibodies (S4B6, Bio X cell). After 4 days, the spleens and LNs of the mice were collected, and single-cell suspensions were prepared and analysed using flow cytometry.

## 2.17 | Pharmacokinetics of EVs

EVs were labelled with $^{64}$Cu as previously described (Warashina et al., 2022). $^{64}$Cu-labelled EVs ($4 \times 10^9$ particles) were intravenously administered to anesthetized recipient mice and PET scans were performed using a Focus 220 MicroPET scanner (Siemens, Knoxville, TN, USA). PET images were reconstructed using MicroPET Manager (version 2.4.1.1; Siemens). The radioactivity of each pixel was decay-corrected from the time of injection and expressed as the standardized uptake value, which was calculated as follows: standardized uptake value = (tissue radioactivity concentration [MBq/cm$^3$])/(injected radioactivity [MBq]/body weight [g]).

## 2.18 | In vivo killing assay

Recipient mice were administered either 200 μg AP-EVs, control EVs, or IL-2/IL-2 mAb. As shown in Figure 4, 4 days following EV administration, the mice were administered splenocytes ($2 \times 10^6$) comprising an equal mix of OVAp-coated CTV-labelled and non-coated CFSE-labelled splenocytes. As shown in Figure 5, 2 days after the third EV administration, mice were administered an equal mixture of CD45.2 OVAp-coated ($1 \times 10^6$) and CD45.1 non-coated splenocytes ($1 \times 10^6$). For both protocols, mouse spleens and LNs were harvested 20 h following splenocyte administration. Single-cell suspensions were prepared from these organs and analysed using flow cytometry.

## 2.19 | Tumour model

To establish the E.G7 tumour model, $1 \times 10^5$ E.G7 cells were subcutaneously inoculated into C57BL/6 mice. The following day, tumour-bearing mice were intravenously administered $1 \times 10^6$ CD45.1 OT-I T cells, followed by 200 μg AP-EVs, control EVs, or IL-2/IL-2 mAb every 3 days starting from day 2, for a total of three administrations. The inoculation procedure was similar

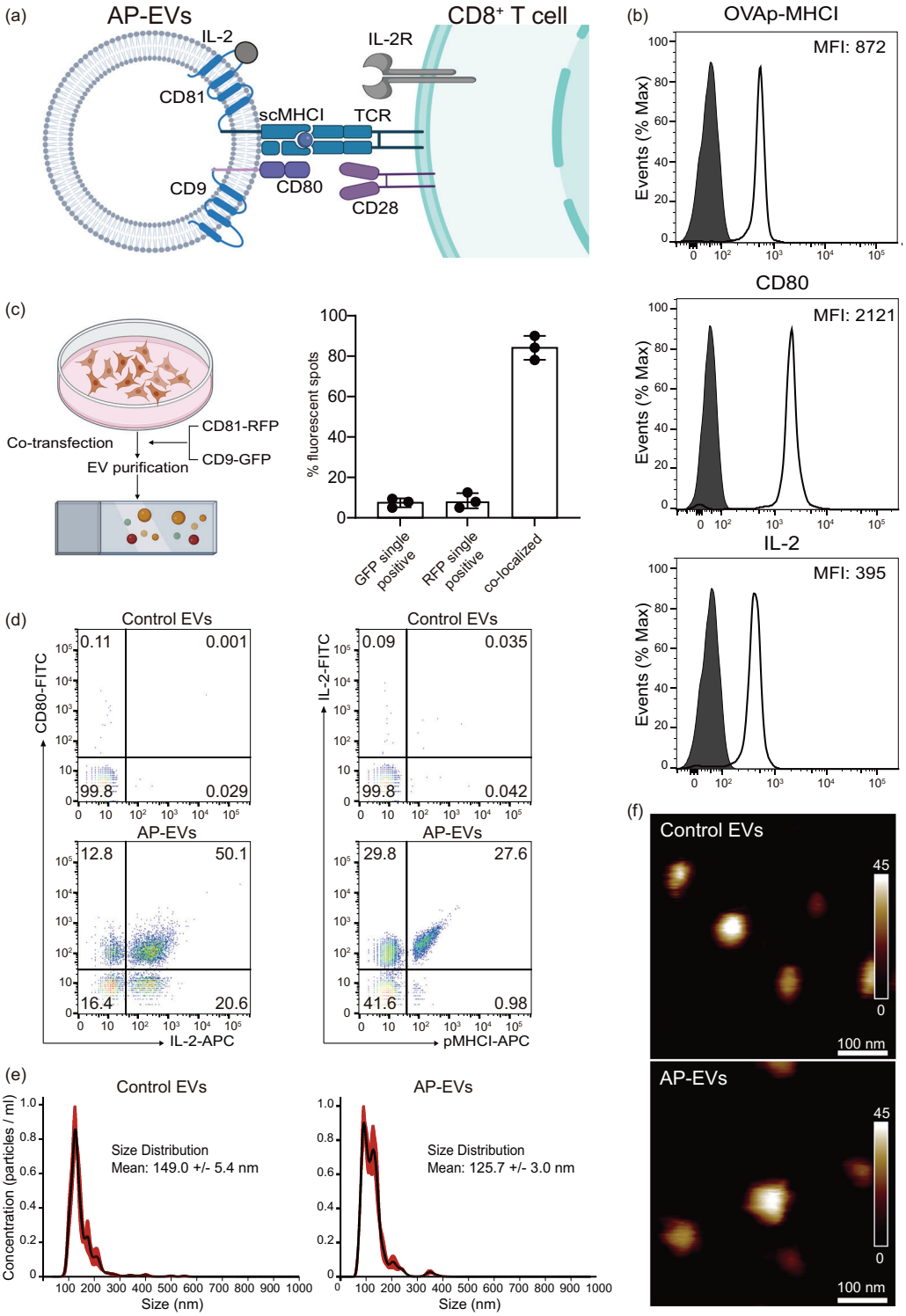


**FIGURE 1** Establishment of antigen-presenting EVs (AP-EVs). (a) Schematic representation of AP-EVs. The functional pMHCI complex, CD80 and IL-2 on AP-EVs interact with TCR, CD28 and IL-2R, respectively, on antigen-specific $CD8^+$ T cells. (b) AP-EV derived from AP-EV stable cell line were captured with Tim4-conjugated beads. Surface expression of the OVAp-MHCI complex, mouse CD80 and mouse IL-2 on EVs was assessed using flow cytometry. Filled grey shapes represent control EVs, and open black shapes represent AP-EVs. MFI was presented in top right corner. (c) HEK293T cells were co-transfected with plasmid expressing CD81-RFP and CD9-GFP fusion protein, and EVs were isolated with ultracentrifugation and observed via confocal microscopy. Colocalization of RFP and GFP positive dot was quantified. (d) EVs isolated from the AP-EV stable cell line or HEK293T cells were stained with fluorescence-conjugated antibodies. Signal expression on single EVs was analysed by NanoFCM. The upper left dot plot shows control EVs stained for IL-2 and CD80, lower left dot plot shows AP-EVs stained for IL-2 and CD80, the upper right dot plot shows control EVs stained for pMHCI and IL-2, and the lower right dot plot shows AP-EVs stained for pMHCI and IL-2. (e) Size distribution between control EVs and AP-EVs (red-shaded region = standard error of the mean). (f) AFM showing AP-EV and control EV morphology (scale bar = 100 nm). Data (b–f) are representative of two independent experiments. AFM, Atomic force microscopy; AP-EV, antigen-presenting EV; EV, extracellular vesicle; GFP, green fluorescent protein; RFP, red fluorescent protein; TCR, T cell receptor.

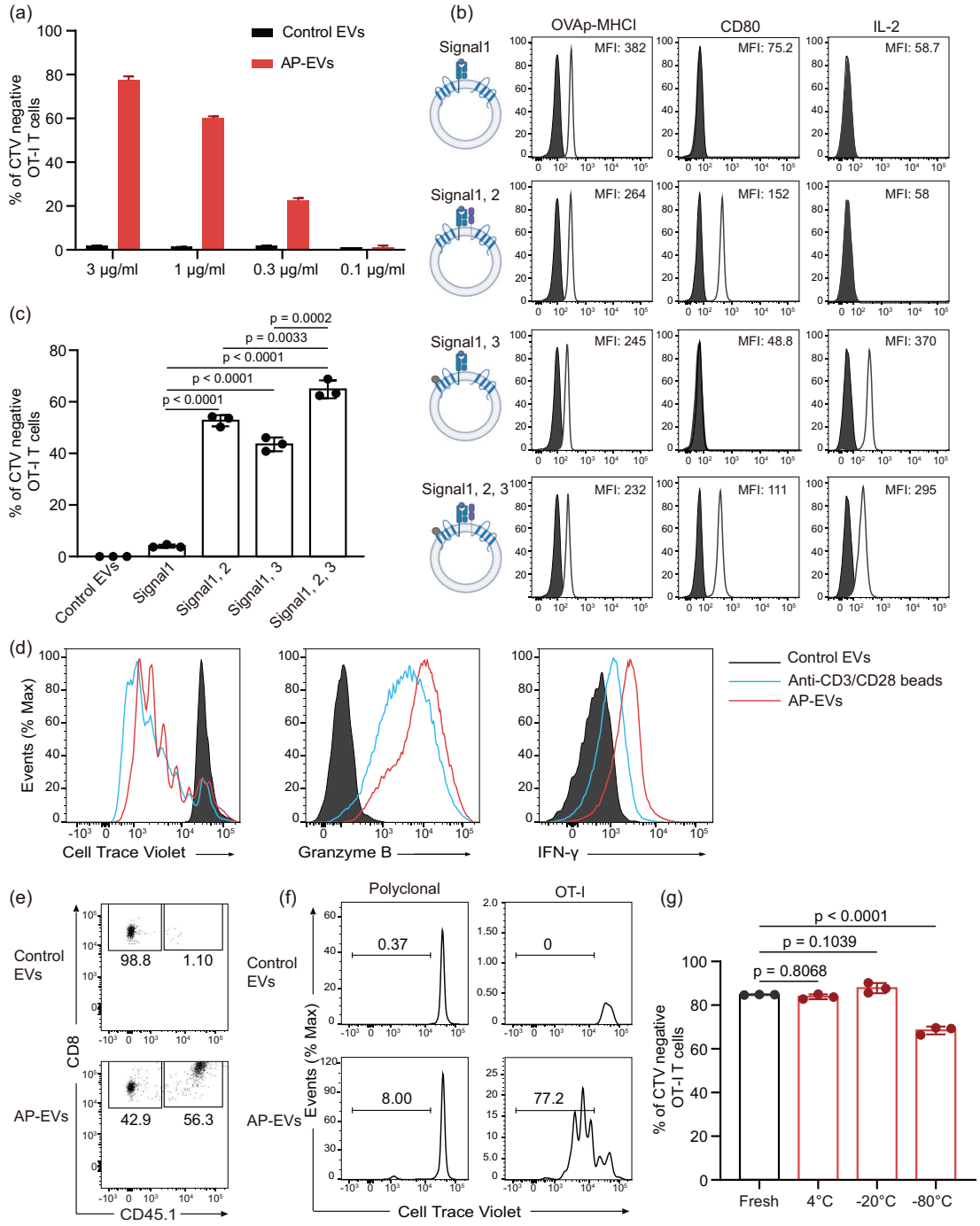


**FIGURE 2** Direct activation of antigen-specific CD8$^+$ T cells by AP-EVs. (a) CTV labelled OT-I T cells were cocultured with AP-EV or control EV. Bar graph representing the percentage of CTV-negative OT-I T cells under different concentrations of control EVs (black) and AP-EVs (red). (b) Surface expression of the OVAp-MHCI complex, CD80 and IL-2 on EVs presented as different signals (alone and in combination). MFI was presented in top right corner. (c) Stimulatory capability of EVs expressing individual signals (1, 2 and 3). CTV-labelled OT-I T cells were cultured with each EV type prepared in (b); the percentage of CTV-negative OT-I T cells was quantified using flow cytometry. *p*-Values were calculated using one-way ANOVA followed by Dunnett's test. Dots represent technical triplicate. (d) Production of granzyme B and IFN-$\gamma$ by CTV-labelled OT-I T cells cultured with AP-EVs, control EVs or anti-CD/3CD28 beads for 3 days were determined by intracellular staining. (e) Flow cytometric plots of CTV-labelled OT-I T (CD45.1) and polyclonal T cells (CD45.2) cultured with either AP-EVs or control EVs for 3 days. Numbers represent the percentage of OT-I T cells and polyclonal T cells. (f) Proliferation of OT-I and polyclonal T cells after culturing with control EVs or AP-EVs determined by flow cytometry. Numbers represent the percentage of CTV-negative CD8$^+$ T cells. (g) Percentage of CTV-negative OT-I after culturing with AP-EVs stored at 4°C, −20°C and −80°C for 3 months or freshly prepared AP-EVs determined by flow cytometry. Dots represent technical triplicate. *p*-Values were determined in (c) and (g) using one-way ANOVA followed by Dunnett's test. Data (a–g) are representative of two independent experiments. ANOVA, analysis of variance; AP-EV, antigen-presenting EV; CTV, cell trace violet; EV, extracellular vesicle.

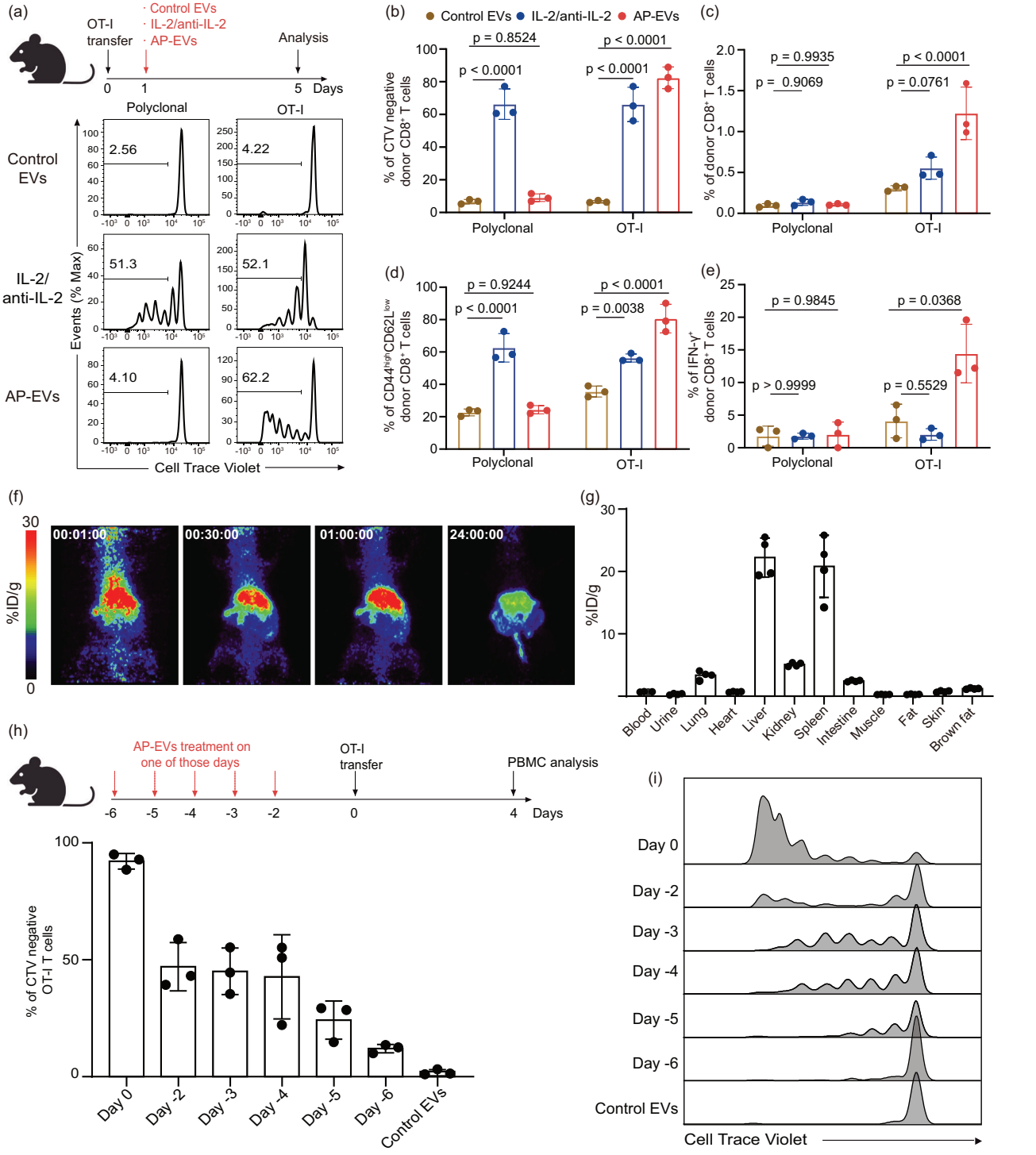


**FIGURE 3** In vivo activation of antigen-specific CD8$^+$ T cells by AP-EVs. (a) CTV-labelled OT-I (CD45.1) and polyclonal T cells (CD45.2) were inoculated into CD45.1$^+$CD45.2$^+$ recipient mice. The following day, mice were administered either control EVs, IL-2/anti-IL-2 mAb or AP-EVs ($n = 3$ mice per group). Numbers represent the percentage of CTV-negative OT-I T cells and polyclonal T cells in spleen 4 days after treatment. (b) Percentage of CTV-negative donor CD8$^+$ T cells in the spleen ($n = 3$ mice per group). (c) Proportion of donor CD8$^+$ T cells among total CD8$^+$ T cells in the spleen ($n = 3$ mice per group). (d) Percentage of CD44$^{high}$CD62L$^{low}$ cells among the splenic CD8$^+$ T cells ($n = 3$ mice per group). (e) Proportion of IFN-$\gamma^+$ cells in the spleen ($n = 3$ mice per group). *p*-Values were calculated using two-way ANOVA (b-e) followed by Tukey's test. (f) Pharmacokinetic studies of AP-EVs. Representative MIP positron emission tomography images are shown at 1 min, 30 min, 1 h, and 24 h post-injection of AP-EVs. (g) Average radioactivity concentration across tissues presented as the percentage of injected dose per gram tissue (%ID/g) after 24.5 h ($n = 4$ mice per group). (h,i) Recipient mice were treated with AP-EVs prior to OT-I T cell transfer at specific intervals. After 4 days, the proliferation of OT-I T cells was quantified ($n = 3$ mice per group). Data (a-i) are representative of two independent experiments. ANOVA, analysis of variance; AP-EV, antigen-presenting EV; EV, extracellular vesicle; MIP, maximum intensity projection.

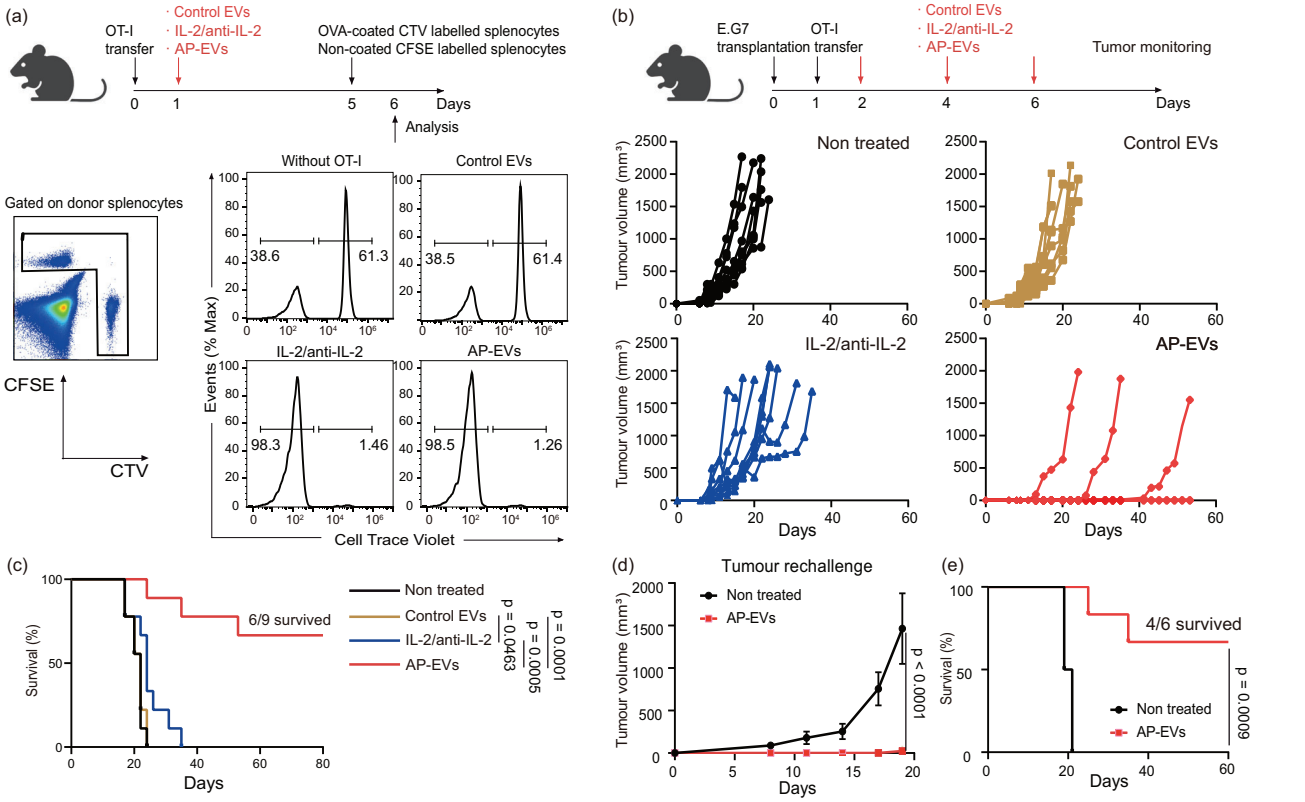


**FIGURE 4** Effect of AP-EV administration on anticancer immunity. (a) Experimental workflow of the in vivo killing assay. $CD45.1^+CD45.2^+$ recipient mice were treated with $CD45.1^+$ OT-I T cells and injected with either control EVs, IL-2/anti-IL-2 mAb or AP-EVs. The survival of donor CTV-labelled OVAp-pulsed $CD45.2^+$ and CFSE-labelled non-pulsed $CD45.2^+$ splenocytes was assessed 20 h after infusion. Data are presented as the ratio of OVAp-pulsed (CTV-labelled) to non-pulsed splenocytes ($n = 3$ mice per group). (b) E.G7 cells were transplanted into recipient mice, followed after 1 day by three treatments with either control EVs, IL-2/anti-IL-2 mAb or AP-EVs at 3 days intervals. Tumour growth curves represent the untreated (black), control EV (brown), IL-2/anti-IL-2 mAb (blue) and AP-EV (red) groups ($n = 9$ mice per group). (c) Kaplan–Meier survival curve of overall survival. Statistical analysis was performed using a log-rank (Mantel–Cox) test ($n = 9$ mice per group). (d) Mice that previously rejected E.G7 post-AP-EV treatment were later subcutaneously challenged with $1 \times 10^5$ E.G7 cells. The tumour growth curves compare untreated and AP-EV-treated mice. *p*-Values were determined using two-way ANOVA followed by Dunnett's test. (e) Kaplan–Meier survival curve for mice subjected to tumour rechallenge. Statistical analysis was performed using a log-rank (Mantel–Cox) test ($n = 6$ mice per group). Data (a-c) are representative of two independent experiments. ANOVA, analysis of variance; AP-EV, antigen-presenting EV; CTV, cell trace violet; EV, extracellular vesicle.

to that used for the tumour model established without adoptive OT-I T cell transfer; however, treatment was initiated on day 1 post E.G7 cell inoculation. Tumour volumes were measured every 2–3 days using a digital caliper and were calculated as length (mm) × width$^2$ (mm$^2$) × 0.5. Prior to the anti-PD1 combination therapy, E.G7 cells were subcutaneously injected into the mice. Treatment was initiated when tumour size reached 50–100 mm$^3$. Mice were randomly allocated to one of four groups depending on the treatment, including 200 μg AP-EVs, control EVs, anti-PD1 antibody and combination therapy groups. The 200 μg AP-EV/control EV and anti-PD1 treatments were administered every 3 days for a total of three administrations and tumour volume measurements and calculations were performed for each mouse. For the tumour rechallenge model, mice that remained tumour-free for 60 days after initial tumour inoculation, and age-matched wild-type mice, were subcutaneously inoculated with $1 \times 10^5$ E.G7 cells without any further treatment. Tumour volume was measured in both groups at 2 or 3 days intervals.

## 2.20 | TIL analysis

E.G7 cells ($1 \times 10^5$) were subcutaneously inoculated into C57BL/6 mice. The following day, tumour-bearing mice were intravenously administered 200 μg AP-EVs, control EVs, or IL-2/anti-IL-2 mAb every 3 days, for a total of three administrations. On day 18, tumours were isolated and TILs were prepared using a Tumor Dissociation Kit (Miltenyi Biotec) according to the manufacturer's instructions. To measure IFN-$\gamma$ production, $5 \times 10^5$ TILs were stimulated overnight with 10 μM OVA peptide, treated with brefeldin A for 5 h, harvested, surface-stained, fixed, and permeabilized using the True-Nuclear Transcription Factor Buffer Set (BioLegend). The cells were stained with anti-IFN-$\gamma$ antibody.

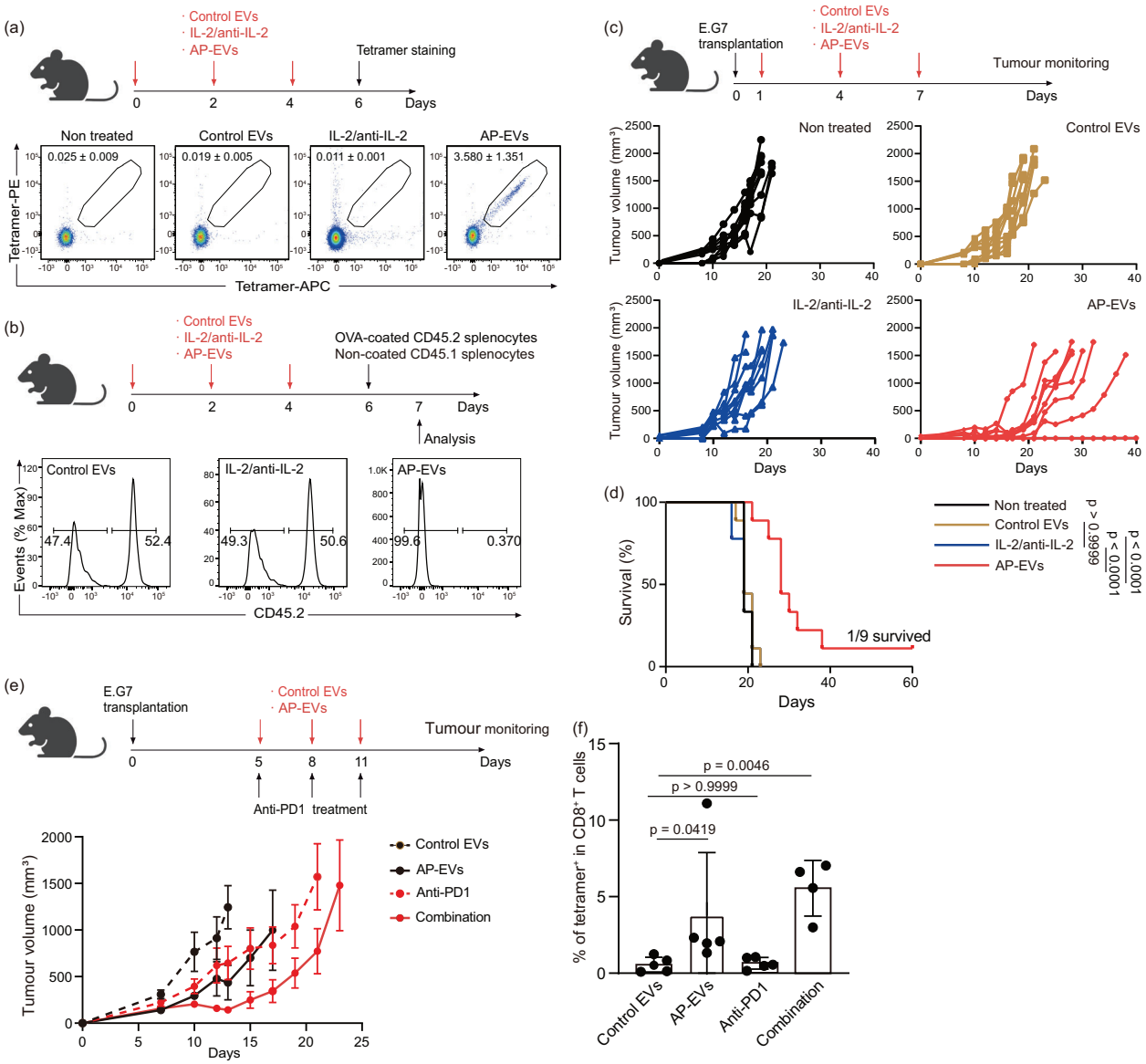


**FIGURE 5** Effect of AP-EVs on the expansion of endogenous antigen-specific $CD8^+$ T cells and cancer immunity. (a) Mice were treated with either 200 μg control EVs, IL-2/anti-IL-2 mAb or 200 μg AP-EVs for three times in a 2 days interval. On day 6, PBMCs were collected. Dots showed the percentages of tetramer-positive cells ($n = 4$). Standard deviation was presented in top left corner. (b) Experimental workflow for the in vivo killing assay. Mice were treated with either 200 μg control EVs, IL-2/anti-IL-2 mAb or 200 μg AP-EVs for three times in a 2 days interval. On day 6, OVAp-pulsed ($CD45.2^+$) with non-pulsed ($CD45.1^+$) splenocytes were transferred to recipient mice. The ratios displayed the percentage of OVAp-pulsed ($CD45.2^+$) with non-pulsed ($CD45.1^+$) splenocytes in recipient mice's PBMCs. (c) E.G7 cells were inoculated into recipient mice, followed after 1 day by three treatments with either 200 μg of control EVs, IL-2/anti-IL-2 mAb or AP-EVs for three times at 3 days intervals. The tumour growth curves are shown. (d) Kaplan–Meier survival curve depicting overall survival rates. Statistical analysis was performed using a log-rank (Mantel–Cox) test ($n = 9$ mice per group). (e) Starting from day 5 (tumour size approximately 100 $mm^3$), E.G7 tumour-bearing mice were treated three times at 3 days intervals with 200 μg of control EVs, AP-EVs, 200 μg of anti-PD1 antibody or a combination of AP-EVs and anti-PD1 antibody for three times. The tumour growth curves are shown. (f) OVAp-specific $CD8^+$ T cells in PBMCs were detected on day 14. Percentages of tetramer-positive cells from tumour-bearing mice treated with control EVs, AP-EVs, anti-PD1 antibody or AP-EVs with anti-PD1 antibody are presented ($n = 5$ mice per group). *p*-Values were calculated using one-way ANOVA followed by Tukey's test. Data (a-f) are representative of two independent experiments. ANOVA, analysis of variance; AP-EV, antigen-presenting EV; EV, extracellular vesicle; PBMC, peripheral blood mononuclear cell.

## 2.21 | Assessment of AP-EV safety in mice

Six- to eight-week-old female C57BL/6 mice were treated with 200 μg of AP-EV or control EVs three times at 3 days intervals. At 1- and 14 days post-treatment, liver and lung tissues were collected for Hematoxylin and Eosin (H&E) staining and Sirius Red staining to quantify inflammation and fibrosis. To measure liver enzymes (aspartate aminotransferase (AST) and alanine aminotransferase (ALT)) and kidney function markers (blood urea nitrogen (BUN) and creatinine (CRE)), 200 μL of peripheral

blood was collected from the mouse tail after the completion of the three-dose treatment regimen (200 μg of AP-EV or control EVs administered at 3 days intervals) at 1- and 14 days post-treatment. The collected blood was incubated at room temperature for 1 h, and then centrifuged at 500 × *g* for 4 min to obtain serum. Assays were performed according to the manufacturers' instructions as follows: AST Activity Assay Kit (Sigma-Aldrich), AST Activity Assay (Sigma-Aldric), BUN Colorimetric Detection Kit (Thermo Fisher), and Creatinine Colorimetric Assay Kit (Cayman).

### 2.22 | TCR transduction of primary human T cells and co-culture assay with hAP-EVs

To produce humanized AP-EVs, HEK293 cells were genetically modified using the CRISPR-Cas9 system to knock out the expression of β2m. The cells were then transiently transfected with plasmids encoding NY-ESO-1 peptide-single-chain trimer-MFG-E8 and CD80-MFG-E8-IL2 to generate humanized AP-EVs. ICAM1-expressing AP-EVs were generated by co-transfection of plasmids encoding NY-ESO-1 peptide-single-chain trimer-MFG-E8, CD80-MFG-E8-IL2 and ICAM1-MFG-E8. The AP-EVs were enriched by ultracentrifugation. PBMCs from human HLA-A*02:01-positive healthy donors were stimulated with Dynabeads Human T-Activator CD3/CD28 beads (Thermo Fisher Scientific) at a 1:1 ratio in X-VIVO 15 medium (Lonza) supplemented with 5 ng/mL human IL-2 (BioLegend). After 2 days, the beads were removed and the activated T cells were transduced with a lentivirus encoding the NY-ESO-1-specific TCR, which recognizes the NY-ESO-1 peptide sequence p157–165 (SLLMWITQC). The culture medium was changed 3 days post-transduction. On day 5, $1 \times 10^5$ TCR-transduced primary $CD8^+$ T cells (with 40–70% TCR expression) were incubated with 20 or 60 μg/mL of either control EVs, pMHCI complex-expressing EVs, or hAP-EVs in 200 μL X-VIVO 15 medium. After 2 h of cultivation with EVs, cells were harvested, surface-stained, fixed and permeabilized using the True-Nuclear Transcription Factor Buffer Set (BioLegend), followed by staining for Nur77 expression. After 1-day of cultivation with EVs, cells were treated with brefeldin A (BioLegend) for 4 h and stained to investigate CD69 and IFN-γ expression. After 4 days of cultivation with EVs, the cell numbers were calculated, cell culture supernatant was collected and secreted granzyme B was measured using a Human Granzyme B ELISA Kit (Abcam) or intracellular staining using antibodies. The assay was performed according to the manufacturer's instructions.

### 2.23 | Statistical analysis

To compare more than two groups, one-way or two-way analysis of variance (ANOVA) was applied. The variation in survival rates was analysed using log-rank tests. All statistical analyses were performed using GraphPad Prism version 8.0 (GraphPad Software, San Diego, CA, USA). $p < 0.05$ was considered statistically significant.

## 3 | RESULTS

### 3.1 | Simultaneous expression of immune modulators on EVs

To present the protein of interest on the surface of EVs, we employed fusion with tetraspanins, such as CD9 or CD81 (Figure 1a) (Stickney et al., 2016). First, we designed the CD81 fusion protein with a single-chain MHCI trimer (scMHCI) consisting of an ovalbumin (OVA) peptide, β2m and H2-$K^b$ molecule (Figure S1a) (Hansen et al., 2010). We integrated IL-2 into the second extracellular loop of CD81 via a GS linker to ensure its robust and functional presentation on the EVs (Figure S1a,b). Concurrently, CD80 was fused with CD9 (Figure S1c). Subsequently, EVs were harvested from the supernatant of human embryonic kidney (HEK293) cells that stably expressed scMHCI-CD81-IL-2 and CD80-CD9. Flow cytometry revealed high levels of OVAp-MHCI, CD80 and IL-2 on the EVs from HEK293 cells (Figure 1b), which we named AP-EVs. Western blot analysis confirmed both the presence of fusion proteins in AP-EVs and the absence of cellular contaminants such as human β-actin and human glyceraldehyde 3-phosphate dehydrogenase (GAPDH), verifying the purity of our EV preparation (Figure S1d) (Théry et al., 2018). To verify the concurrent expression of CD9 and CD81 fusion proteins on individual EVs, HEK293T cells were co-transfected with CD9-green fluorescent protein (GFP) and CD81-red fluorescent protein (RFP) constructs, and EVs were isolated from the culture supernatant. Consistent with prior observations (Corso et al., 2019) confocal microscopy revealed that ~80% of the EVs co-expressed GFP and RFP (Figure 1c, Figure S1e), suggesting that the majority of AP-EVs simultaneously display OVAp-MHCI-CD81-IL-2 and CD80-CD9. To further validate the co-expression of signals on AP-EVs, we also confirmed the expression of scMHCI-CD81-IL-2 and CD9-CD80 by NANO-FCM, a state-of-the-art flow cytometer that analyses individual EVs, and found that over 50% of the EVs co-expressed IL-2 and CD80 (Figure 1d). On the other hand, when we analysed MHCI and IL-2 co-expression in our control experiment, we did not observe 100% co-expression of these proteins despite all EVs theoretically expressing both molecules (Figure 1d). This discrepancy likely reflects technical limitations in single EV flow cytometry detection, such as antibody competition. Therefore, the observed 50% co-localization of IL-2 and CD80 may represent an underestimate of the actual co-expression levels. Nanoparticle tracking analysis showed that the average size of AP-EVs was ~150 nm, comparable to that of

non-modified control EVs (Figure 1e); transmission electron microscopy revealed that AP-EVs exhibited typical vesicular morphology characteristic of EVs (Figure S1f), and atomic force microscopy (AFM) showed that AP-EVs had morphological and physical properties similar to those of control EVs (Figure 1f, Figure S1g,h).

## 3.2 | Selective expansion of antigen-specific CD8$^+$ T cells with AP-EVs

DC-derived exosomes can directly prime effector T cells but are ineffective in stimulating naïve T cells (Segura et al., 2005; Théry et al., 2002). We investigated if AP-EVs can stimulate naïve CD8$^+$ T cells; therefore, OVA-specific CD8$^+$ (OT-I) T cells labelled with cell trace violet (CTV) were cultured with various doses of AP-EVs or control EVs. As naïve T cells lose CTV staining upon activation, we measured the percentage of CTV-negative T cells to assess activation and proliferation. After 3 days of cultivation, a dose-dependent expansion of OT-I T cells was observed with AP-EV treatment (Figure 2a, Figure S2). This indicated that AP-EVs directly activated naïve CD8$^+$ T cells. Subsequently, we examined the minimally required components (signal 1: OVAp-MHCI, signal 2: CD80, signal 3: IL-2) on AP-EVs for T cell activation. We prepared EVs expressing signal 1 alone; signals 1 and 2; signals 1 and 3; or signals 1, 2 and 3 (Figure 2b) and co-cultured them with OT-I T cells. Signal 1-expressing EVs did not efficiently activate OT-I T cells (Figure 2c). In contrast, co-expression with signals 2 or 3 strongly stimulated the proliferation of OT-I T cells, and co-expression of signals 1, 2 and 3 showed the maximum effect. This indicated that signals 2 and 3 synergistically enhanced CD8$^+$ T cell expansion. Moreover, using anti-CD3/CD28 beads as a positive control for T cell activation, AP-EVs were shown to activate OT-I T cells, leading to the production of IFN-$\gamma$ and granzyme B. This suggests the differentiation of naïve T cells into cytotoxic T lymphocytes (CTLs) (Figure 2d). To determine whether AP-EVs could specifically stimulate CD8$^+$ T cells, OT-I T cells (CD45.1$^+$) were co-cultured with polyclonal CD8$^+$ T cells (CD45.2$^+$) at a 5:95 ratio, and either control EVs or AP-EVs were added to the culture. Although control EVs maintained the initial ratio of OT-I to polyclonal CD8$^+$ T cells, AP-EVs selectively expanded the OT-I T cell population in vitro (Figure 2e,f). Although we utilized freshly isolated AP-EVs, we observed that AP-EVs stored for up to 3 months at 4°C or −20°C (but not −80°C) demonstrated activity comparable to that of fresh EVs (Figure 2g). Collectively, these results indicated that AP-EVs, which directly present an antigen, costimulatory molecule and cytokine, induce robust proliferation of antigen-specific CD8$^+$ T cells.

## 3.3 | In vivo expansion of antigen-specific CD8$^+$ T cells by AP-EVs

IL-2/anti-IL-2 mAb complexes selectively bind IL-2R$\beta$ and $\gamma$, promoting the expansion of CD8$^+$ T and NK cells; however, their use for in vivo CD8$^+$ T cell expansion often results in non-specific CD8$^+$ T cell activation and side effects such as splenomegaly (Boyman et al., 2006). To effectively deliver IL-2 to antigen-specific CD8$^+$ T cells in vivo without causing severe adverse effects, we investigated the ability of AP-EVs to selectively stimulate antigen-specific CD8$^+$ T cells. Accordingly, we transferred a mixture of congenically marked OT-I T and polyclonal T cells (1:1) to recipient CD45.1$^+$CD45.2$^+$ mice, followed by intravenous injection of AP-EVs, control EVs or IL-2/anti-IL-2 mAb. After 4 days, donor T cells were analysed (Figure 3a). Consistent with a previous finding (Létourneau et al., 2010), the IL-2/anti-IL-2 mAb expanded both OT-I and polyclonal T cells. In contrast, AP-EVs exhibited selective expansion of OT-I T cells in the spleen (Figure 3a–c) and lymph nodes (LNs) (Figure S3a–c), with the majority of OT-I T cells acquiring the CD44$^{high}$CD62L$^{low}$ effector memory or effector phenotype (Figure 3d, Figure S3d). Additionally, a subset of OT-I T cells differentiated into IFN-$\gamma$ positive CTLs (Figure 3e, Figure S3e). To investigate the in vivo distribution of AP-EVs, we conducted a pharmacokinetic analysis of $^{64}$Cu-labelled AP-EVs using positron emission tomography (PET) imaging (Warashina et al., 2022) and found that AP-EVs predominantly accumulated in the spleen and liver (Figure 3f,g). To clarify the functional duration of AP-EVs in vivo, we administered them several days prior to the transfer of OT-I T cells. Although a substantial fraction of AP-EVs was cleared by day 2, sufficient activating capacity remained until day 4 after AP-EV administration (Figure 3h,i).

## 3.4 | AP-EVs potentiate the anticancer efficiency of adoptively transferred T cells

We determined whether the OT-I T cell expansion following the AP-EV treatment in mice could specifically eliminate OVAp-coated splenocytes by introducing a mixture of CTV-labelled OVAp-coated and CFSE-labelled non-coated splenocytes (1:1) 4 days after EV administration. A marked reduction in OVAp-coated splenocytes from ∼60% to 1.26% indicated that AP-EV-activated CTLs had high antigen-specific cytotoxicity (Figure 4a). To evaluate their tumour-killing activity, we subcutaneously inoculated OVA-expressing EL4 (E.G7) cells in mice, followed by the injection of OT-I T cells after 1 day and three doses of AP-EVs, control EVs or IL-2/anti-IL-2 mAb (Figure 4b). For initial administration, AP-EVs were loaded with pMHCI, CD80 and IL-2. For the two subsequent administrations, we used AP-EVs expressing OVAp-MHCI and IL-2, omitting CD80 to avoid stimulating the inhibitory receptor CTLA-4 (Vandenborre et al., 1999). A previous report indicated that IL-2/anti-IL-2 mAb only induced a marginal delay in cancer growth and limited the extension of survival (Krieg et al., 2010). We found that the administration of AP-EVs significantly delayed cancer progression, and six out of nine mice completely rejected E.G7 cells (Figure 4b,c).

Moreover, mice that rejected E.G7 cells showed pronounced resistance upon subsequent E.G7 cell rechallenge (Figure 4d,e). These findings demonstrated that the administration of AP-EVs stimulates the effector function of antigen-specific CTLs and facilitates the generation of antigen-specific memory $CD8^+$ T cells.

## 3.5 | AP-EVs amplify endogenous antigen-specific $CD8^+$ T cells and enhance anticancer immunity

Approximately 1–100 endogenous $CD8^+$ T cells per million recognize a specific peptide-MHC complex (Jenkins & Moon, 2012). Indeed, the OVA-specific endogenous $CD8^+$ T cells comprise 0.025% of the total $CD8^+$ T cell population in peripheral blood mononuclear cells (PBMCs) from untreated mice (Figure 5a). We investigated the expansion of this rare population in mice following administration with AP-EVs, control EVs, or an IL-2/anti-IL-2 mAb on days 0, 2 and 4. On day 7, the AP-EVs were found to promote the clonal expansion of OVAp-specific $CD8^+$ T cells, representing 3.580% of all $CD8^+$ T cells. In contrast, control EVs or IL-2/anti-IL-2 mAb treatment failed to selectively expand OVAp-specific $CD8^+$ T cells (Figure 5a). We verified the effector function of these expanded OVAp-specific $CD8^+$ T cells through an in vivo killing assay. We introduced a mixture of CD45.2 OVAp-coated and CD45.1 non-coated splenocytes (at a ratio of 1:1) 2 day after the third EV administration. OVAp-coated splenocytes were eliminated from mice that received AP-EVs (Figure 5b), while the control EVs or IL-2/anti-IL-2 mAb had no effect. Furthermore, we investigated whether AP-EVs exert anticancer effects via endogenous CTLs in C57BL/6 mice subcutaneously injected with E.G7 cells and administered AP-EVs, control EVs or IL-2/anti-IL-2 mAb. Notably, the AP-EV treatment resulted in a substantial delay in cancer progression and extension of survival compared with those in the control groups (Figure 5c,d). We explored the efficacy of AP-EVs against established tumours. E.G7 cells were subcutaneously injected into mice and allowed to proliferate until reaching a size of 100 $mm^3$. The mice were administered AP-EVs, anti-PD-1 antibodies or a combination of both. Monotherapy using either AP-EVs or anti-PD-1 antibodies resulted in only a slight delay in tumour progression, whereas combination therapy markedly inhibited tumour growth (Figure 5e). Notably, we observed an increased percentage of antigen-specific $CD8^+$ T cells among the total $CD8^+$ T cells, reflecting a synergistic effect between AP-EVs and the anti-PD-1 antibody (Figure 5f). These findings highlight the effectiveness of AP-EVs not only in the selective expansion of endogenous antigen-specific $CD8^+$ T cells but also in enhancing anticancer immunity, particularly when employed with an anti-PD-1 immune checkpoint inhibitor. Moreover, we evaluated the toxicity of AP-EVs and found that their administration did not present any apparent adverse effects: we observed no marked changes in body weight, no tissue abnormalities and blood chemistry parameters consistent with those of the vehicle-treated controls (Figure S4). Additionally, no expansion of polyclonal $CD4^+$ T cells, polyclonal $CD8^+$ T cells, NK cells or Tregs was observed (Figure S5).

## 3.6 | AP-EVs accumulate in the tumour microenvironment

To investigate the effects of AP-EVs on the tumour microenvironment and their potential contribution to enhanced anticancer immunity, we performed a tumour-infiltrating lymphocyte (TIL) analysis (Figure 6a). We observed the accumulation of $CD8^+$OVAp-tetramer$^+$ cells (Figure 6b), an increased percentage of IFN-$\gamma^+$ $CD8^+$ T cells (Figure 6c), and a decreased percentage of OVAp-tetramer$^+$PD-$1^+$ exhausted $CD8^+$ T cells (Figure 6d), suggesting that administration of AP-EVs turned the 'cold' tumour microenvironment into a 'hot' one. We analysed the distribution of $^{64}$Cu-labelled AP-EVs in untreated and E.G7 tumour-bearing C57BL/6 mice, and the accumulation of AP-EVs was evaluated 24 h after administration. Similar to the results in Figure 3f, we observed the hepatic accumulation of AP-EVs along with marked accumulation in the tumour (Figure 6e), which increased over time (Figure 6f). These results suggested that AP-EVs may activate antigen-specific $CD8^+$ T cells in situ, both within the tumour microenvironment and secondary lymphoid organs.

## 3.7 | Humanized AP-EVs stimulate primary human $CD8^+$ T cells

To create humanized AP-EVs (hAP-EVs), we utilized milk fat globule epidermal growth factor 8 (MFG-E8), which binds phosphatidylserine (PS) on the surface of EV and is commonly used for EV engineering (Dooley et al., 2021). We engineered the MFG-E8 fusion protein with a scMHCI comprising an NY-ESO-1 peptide, $\beta$2m and the HLA-A02:01 molecule (Figure 7a, Figure S6a). hCD80 was fused with MFG-E8 and hIL-2 (Figure 7b, Figure S6b). Flow cytometry revealed that hAP-EVs expressed $\beta$2m, hCD80 and hIL-2 (Figure 7c). To assess the functionality of hAP-EVs, we transduced PBMCs from a single HLA-A02:01-positive healthy volunteer with a lentiviral vector carrying the NY-ESO-1 peptide-specific T cell receptor (TCR) (Robbins et al., 2008), which also contained a 2A peptide sequence and Venus reporter for the efficient tracking and analysis of $CD8^+$ T cells expressing NY-ESO-1 peptide-specific TCR. After transduction, 40%–70% of the $CD8^+$ T cells expressed Venus, most of which were positive for NY-ESO-1p tetramer staining (Figure 7d). After 2 h of cultivation with hAP-EVs, TCR-positive cells showed higher levels of Nur77, a marker of TCR signalling events (Ashouri & Weiss, 2017) than TCR-negative cells, whereas no change in expression was observed in cells cultured with control EVs or those expressing only the pMHCI complex (Figure 7e). This activation was further

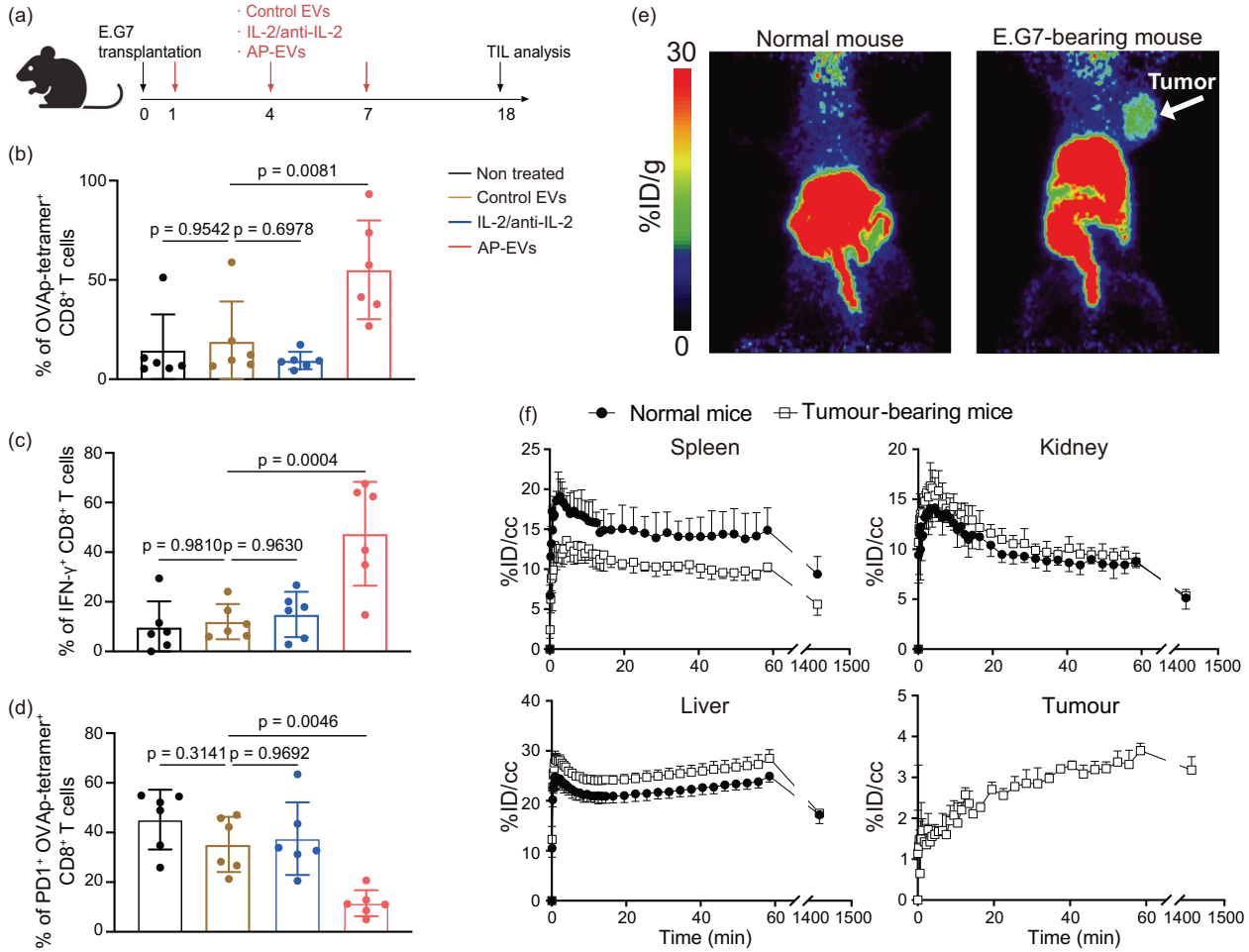


**FIGURE 6** AP-EVs can directly activate TILs. (a) Schematic representation of AP-EV administration protocol. E.G7 cells were inoculated into recipient mice. The following day, mice received three treatments with either 200 μg control EVs, IL-2/anti-IL-2 mAb or 200 μg AP-EVs for three times at 3 days intervals. TILs were harvested on day 18 ($n = 6$ mice per group). (b) Percentage of $CD8^+$OVAp-$tetramer^+$ cells in TILs. (c) Percentage of IFN-$\gamma^+$ $CD8^+$ T cells in TILs. (d) Percentage of OVAp-$tetramer^+$PD-$1^+$ exhausted $CD8^+$ T cells. *p*-Values were calculated using one-way ANOVA followed by Dunnett's test. (e) $^{64}$Cu-labelled AP-EVs were administered to untreated and E.G7 tumour-bearing C57BL/6 mice. AP-EV accumulation was evaluated 24 h following administration. (f) Time-activity curve presenting the percentage injected dose per cubic centimetre of tissue (%ID/cc). Data (a-f) are representative of two independent experiments. ANOVA, analysis of variance; AP-EV, antigen-presenting EV; TIL, tumour-infiltrating lymphocytes.

characterized by elevated CD69 expression and IFN-$\gamma$ and granzyme B production (Figure 7f–h). Additionally, the number of NY-ESO-1 peptide-specific $CD8^+$ T cells increased after cultivation with hAP-EVs for 4 days (Figure 7i). To further enhance their T cell activation capacity, we modified hAP-EVs with the ICAM-1 adhesion molecule and found that they more efficiently stimulated NY-ESO-1 peptide-specific $CD8^+$ T cells than hAP-EVs alone (Figure S7). Collectively, these results demonstrated that hAP-EVs effectively stimulate primary human $CD8^+$ T cells in vitro, which was further enhanced by the incorporation of ICAM-1 into hAP-EVs.

## 4 | DISCUSSION

Nanoparticles and EVs, including exosomes, have attracted widespread attention for their potential as drug delivery systems, diagnostic tools, tissue regenerative agents and immune response modulators. They offer several advantages, including a low risk of entrapment in small blood vessels, minimal risk of malignant transformation and increased stability compared with cell-based therapies. Hence, various studies have engineered nanoparticles and EVs capable of activating immune responses. For example, nanoparticles conjugated with pMHCI and costimulatory molecules or anti-CD28 antibody can effectively expand antigen-specific $CD8^+$ T cells (Ben-Akiva et al., 2023; Hickey et al., 2017). Despite their remarkable extensibility, the non-biological origin of nanoparticles presents potential issues in terms of biocompatibility and may elicit undesirable immune responses or toxicity in clinical applications. In contrast, EVs naturally exhibit superior biocompatibility owing to their bio-

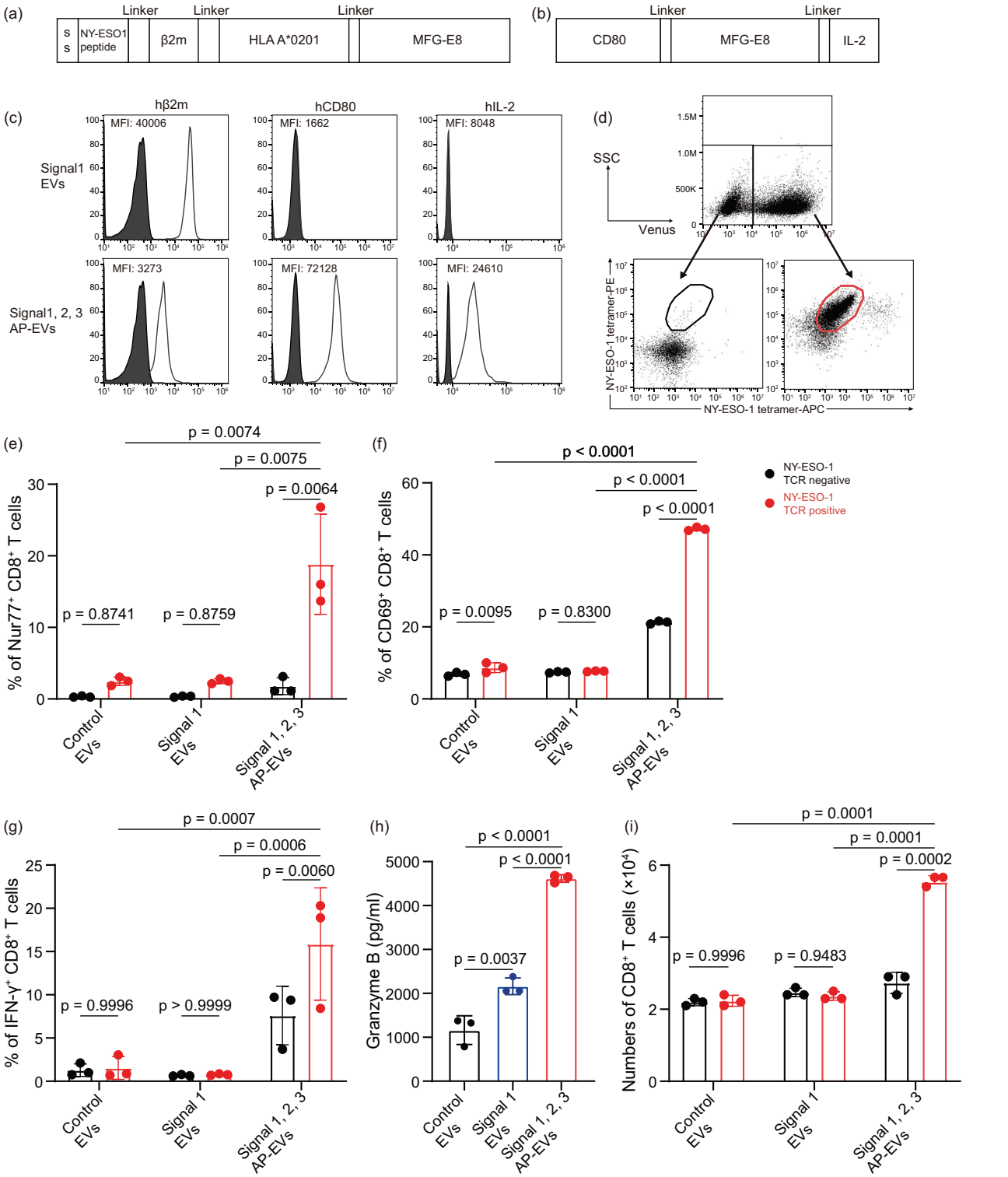


**FIGURE 7** Induction of human antigen-specific T cell expansion, activation and effector function by AP-EVs in vitro. (a) Schematic illustration of NY-ESO-1 single-chain trimer-MFG-E8 fusion protein. (b) Schematic illustration of CD80-MFG-E8-IL2 fusion protein. (c) Human β2m-deficient 293 cells were transiently transfected with NY-ESO-1 single-chain trimer-MFG-E8 fusion protein or co-transfected with NY-ESO-1 single-chain trimer-MFG-E8 fusion protein and CD80-MFG-E8-IL2 fusion protein. EVs were captured with Tim4-conjugated beads. Histogram figures show the expression of human β2m, CD80 and IL-2 on EVs. Upper panels show EVs isolated from NY-ESO-1 single-chain trimer-MFG-E8 fusion protein transfected β2m-deficient 293 cells. The bottom panels show EVs isolated from NY-ESO-1 single-chain trimer-MFG-E8 fusion protein and CD80-MFG-E8-IL2 fusion protein co-transfected β2m-deficient 293 cells. MFI was presented in top left. (d) PBMCs were transduced with NY-ESO-1 TCR via lentiviral transfection. Representative dot plots showing NY-ESO-1 tetramer staining in NY-ESO-1 TCR (Venus)-positive and Venus-negative human $CD8^+$ T cells. (e) Nur77 expression in NY-ESO-1 TCR-positive

*(Continues)*

**FIGURE 7** (Continued)

and NY-ESO-1 TCR-negative T cells after 2 h of stimulation with AP-EVs, signal 1 expressing EVs or control EVs (prepared in c). (f) Percentage of $CD69^+$ NY-ESO-1 TCR-positive and NY-ESO-1 TCR-negative T cells after 1 day of stimulation with 60 μg/mL AP-EVs, signal 1 expressing EVs or control EVs. (g) IFN-$\gamma$ expression in NY-ESO-1 TCR-positive and TCR-negative $CD8^+$ T cells following 1 day of stimulation with 60 μg/mL AP-EVs, signal 1 expressing EVs or control EVs. (h) Amount of granzyme B in the supernatant after 4 days of co-culture determined by ELISA. (i) Numbers of NY-ESO-1 TCR-positive T and NY-ESO-1 TCR-negative T cells following 4 days of stimulation with 60 μg/mL AP-EVs, signal 1 expressing EVs or control EVs. *p*-Values were calculated using two-way ANOVA (e, f, g, i) and one-way ANOVA (h) followed by Tukey's test. Data (e–i) are presented as technical triplicates. Data (c–i) are representative of two independent experiments. ANOVA, analysis of variance; AP-EV, antigen-presenting EV; EV, extracellular vesicle; PBMC, peripheral blood mononuclear cell; TCR, T cell receptor.

logical origins. We engineered AP-EVs equipped with multiple immune modulators on a single EV platform. This design allows for the concurrent stimulation of targeted T cells with TCR, costimulatory and cytokine signals. A key advantage of AP-EVs is their adaptability to modifications, which facilitates the incorporation of a diverse array of cytokines and costimulatory signals. In this study, we integrated IL-2 and CD80 as prototypical cytokines and costimulatory molecules, respectively. However, alternative cytokines and signals, such as IL-12 or 4-1BBL, may also be conceivable. For instance, EVs containing pMHCII, CD80 and IL-12 are anticipated to promote antigen-specific Th1 differentiation, whereas EVs embedded with pMHCII, IL-2 and TGF-$\beta$ may induce antigen-specific Tregs, presenting a potential therapeutic approach for autoimmune regulation (Becker et al., 2023). Additionally, immune checkpoint inhibitors can be applied to AP-EVs to generate anti-PD-1 scFV-tetraspanin fusion proteins (Shi et al., 2020). In the current study, we modified hAP-EVs to express the adhesion molecule ICAM-1 on their surface. Notably, these ICAM-1-bearing hAP-EVs demonstrated an enhanced ability to activate NY-ESO-1 peptide-specific $CD8^+$ T cells compared to the unmodified hAP-EVs. This adaptability in selecting costimulatory molecules, cytokines and other immune modulators enables the flexible customization of AP-EVs for treating various conditions, such as cancer and autoimmune diseases.

DC-based cancer immunotherapies, particularly DC vaccines, are promising therapeutic strategies against malignancies such as acute myeloid leukaemia, myelodysplastic neoplasms and various solid tumours (Anguille et al., 2017; Del Prete et al., 2023). Their ability to present tumour-specific antigens and stimulate robust antitumour responses has increased interest in their clinical use. Although many studies have shown that DC vaccines are safe and feasible, several limitations persist, including undesirable cellular immune responses, high costs and intricate production processes (Sellars et al., 2022). To overcome these limitations, a recent study utilized DC-derived nanovesicles engineered to express pMHCI, costimulatory molecules and an anti-PD-1 antibody (Liu et al., 2022). These nanovesicles effectively activated tumour-specific $CD8^+$ T cells and contributed to antitumour immune responses. However, the nanovesicles lacked cytokine signals and nanovesicle collection from DCs remains challenging. AP-EVs may be a more efficient strategy than DC vaccines or DC-derived nanovesicles owing to their scalable production, ease of modification and inherent stability stemming from their non-cellular composition. Furthermore, the adaptability of AP-EVs allows the integration of key insights from DC vaccine research, such as specific antigen selection, robust immune response stimulation and safety protocols. By leveraging these strategies within the AP-EV design, cancer immunotherapy may be enhanced by combining the strengths of both approaches while overcoming the limitations associated with DC vaccines and DC-derived nanovesicles.

Several cytokines have been modified to boost their functions while avoiding the adverse effects of systemic administration. For example, engineered IL-2 variants have been developed to mitigate the side effects of IL-2 by selectively activating $CD8^+$ memory T and NK cells (Levin et al., 2012; Silva et al., 2019). However, these IL-2 variants lack antigen specificity and cause expansion of the entire $CD8^+$ T cell repertoire. Orthogonal pairs of IL-2/IL-2R offer an alternative approach for specifically targeting T cells (Sockolosky et al., 2018); however, this requires genetic modification of T cells and may inadvertently activate the immune system through repetitive injections because orthogonal IL-2/IL-2R pairs are not recognized as self-antigens. AP-EV technology circumvents these challenges by allowing the selective delivery of IL-2 to antigen-specific T cells owing to the simultaneous surface expression of pMHCI and IL-2 on EVs, which could promote the safety and efficacy of antigen-specific $CD8^+$ T cell activation.

While our study demonstrates the potential of AP-EVs using HLA-A02:01 as a proof of concept, several limitations need to be addressed for clinical application. The high polymorphism of HLA molecules presents a significant challenge, as each individual possesses unique HLA types for antigen presentation. This diversity necessitates the development of personalized AP-EVs expressing specific HLA molecules matching the patient's type to ensure effective antigen presentation. Our current approach using a single HLA allele (HLA-A02:01) was chosen strategically, as this allele is present in approximately half of Western populations. However, for broader clinical applications, establishing a library of AP-EVs with different HLA types or developing patient-specific AP-EVs would be necessary.

## 5 | CONCLUSION

We engineered EVs expressing a suitable costimulatory molecule, cytokine and pMHCI to selectively deliver immune modulators to antigen-specific T cells and inhibit tumour growth and survival. Although our findings confirm the efficacy of

AP-EVs in vivo and in vitro, further research is required to optimize their design and evaluate their safety and efficacy in non-clinical and clinical trials. Overall, our framework for engineering hAP-EVs may greatly advance the development of EV-based immunotherapies.

## AUTHOR CONTRIBUTIONS

**Tomoyoshi Yamano and Rikinari Hanayama**: Conceptualization. **Xiabing Lyu, Tomoyoshi Yamano, and Rikinari Hanayama**: Methodology. **Xiabing Lyu, Tomoyoshi Yamano, Kanto Nagamori, Shota Imai, Toan Van Le, Makie Ueda, Dilireba Bolidong, Shota Warashina, Hidefumi Mukai, Seigo Hayashi, Kazutaka Matoba, and Taito Nishino**: Investigation. **Tomoyoshi Yamano and Rikinari Hanayama**: Supervision. **Xiabing Lyu and Tomoyoshi Yamano**: Writing—original draft. **Xiabing Lyu, Tomoyoshi Yamano, and Rikinari Hanayama**: Writing—review and editing.

## ACKNOWLEDGEMENTS

We thank T. Yoshida for the helpful discussions on this work and Dr. Y. Watanabe, Dr. Y. Wada, and Ms. E. Hayashinaka from RIKEN for their assistance in reconstructing the PET images. We thank I. Minowa and Y. Sato for supporting the management and operation of NanoFCM. This work was supported by the Japan Science and Technology Agency (JST) Precursory Research for Embryonic Science and Technology (PRESTO) [grant no. JPMJPR19HA (T.Y.)]; JST Fusion Oriented Research for Disruptive Science and Technology (FOREST) [grant no. JPMJFR2115 (T.Y.)]; Kanae Foundation for the Promotion of Medical Science and MSD Life Science Foundation, Public Interest Incorporated Foundation (T.Y.); Science and Technology Platform for Advanced Biological Medicine from the Japan Agency for Medical Research and Development (AMED) [grant no. 22am0401019h0004 (R.H.)]; Core Research for Evolutional Science and Technology (CREST) [grant no. JPMJCR18H4 (R.H.)]; and AMED [grant no. JP23ak0101178 (H.M.)].

## CONFLICT OF INTEREST STATEMENT

R.H., T.Y., and K.M. applied for a patent (WO2021172595) on antigen-presenting extracellular vesicles. Other authors confirm that there are no conflicts of interest to declare

## DATA AVAILABILITY STATEMENT

All data are available in the main text and supplemental material. Further information is available from the corresponding author.

## ORCID

*Rikinari Hanayama* https://orcid.org/0000-0003-2102-3386

## REFERENCES

Ahmadzadeh, M., & Rosenberg, S. A. (2006). IL-2 administration increases $CD4^+CD25^{hi}$ $Foxp3^+$ regulatory T cells in cancer patients. *Blood*, *107*, 2409–2414.

Anguille, S., Van de Velde, A. L., Smits, E. L., Van Tendeloo, V. F., Juliusson, G., Cools, N., Nijs, G., Stein, B., Lion, E., Van Driessche, A., Vandenbosch, I., Verlinden, A., Gadisseur, A. P., Schroyens, W. A., Muylle, L., Vermeulen, K., Maes, M. B., Deiteren, K., Malfait, R., … Berneman, Z. N. (2017). Dendritic cell vaccination as postremission treatment to prevent or delay relapse in acute myeloid leukemia. *Blood*, *130*, 1713–1721.

Ashouri, J. F., & Weiss, A. (2017). Endogenous Nur77 is a specific indicator of antigen receptor signaling in human T and B Cells. *Journal of Immunology*, *198*, 657–668.

Atkins, M. B., Lotze, M. T., Dutcher, J. P., Fisher, R. I., Weiss, G., Margolin, K., Abrams, J., Sznol, M., Parkinson, D., Hawkins, M., Paradise, C., Kunkel, L., & Rosenberg, S. A. (1999). High-dose recombinant interleukin 2 therapy for patients with metastatic melanoma: Analysis of 270 patients treated between 1985 and 1993. *Journal of Clinical Oncology*, *17*(7), 2105–2116.

Becker, M. W., Peters, L. D., Myint, T., Smurlick, D., Powell, A., Brusko, T. M., & Phelps, E. A. (2023). Immune engineered extracellular vesicles to modulate T cell activation in the context of type 1 diabetes. *Science Advances*, *9*, eadg1082.

Ben-Akiva, E., Hickey, J. W., Meyer, R. A., Isser, A., Shannon, S. R., Livingston, N. K., Rhodes, K. R., Kosmides, A. K., Warren, T. R., Tzeng, S. Y., Schneck, J. P., & Green, J. J. (2023). Shape matters: Biodegradable anisotropic nanoparticle artificial antigen presenting cells for cancer immunotherapy. *Acta Biomaterialia*, *160*, 187–197.

Berraondo, P., Sanmamed, M. F., Ochoa, M. C., Etxeberria, I., Aznar, M. A., Pérez-Gracia, J. L., Rodríguez-Ruiz, M. E., Ponz-Sarvise, M., Castañón, E., & Melero, I. (2019). Cytokines in clinical cancer immunotherapy. *British Journal of Cancer*, *120*, 6–15.

Besse, B., Charrier, M., Lapierre, V., Dansin, E., Lantz, O., Planchard, D., Le Chevalier, T., Livartoski, A., Barlesi, F., & Laplanche, A. (2016). Dendritic cell-derived exosomes as maintenance immunotherapy after first line chemotherapy in NSCLC. *Oncoimmunology*, *5*, e1071008.

Blanco, E., Shen, H., & Ferrari, M. (2015). Principles of nanoparticle design for overcoming biological barriers to drug delivery. *Nature Biotechnology*, *33*, 941–951.

Boyman, O., Kovar, M., Rubinstein, M. P., Surh, C. D., & Sprent, J. (2006). Selective stimulation of T cell subsets with antibody-cytokine immune complexes. *Science*, *311*, 1924–1927.

Briukhovetska, D., Dörr, J., Endres, S., Libby, P., Dinarello, C. A., & Kobold, S. (2021). Interleukins in cancer: From biology to therapy. *Nature Reviews Cancer*, *21*, 481–499.

Chen, G., Huang, A. C., Zhang, W., Zhang, G., Wu, M., Xu, W., Yu, Z., Yang, J., Wang, B., Sun, H., Xia, H., Man, Q., Zhong, W., Antelo, L. F., Wu, B., Xiong, X., Liu, X., Guan, L., Li, T., … Guo, W. (2018). Exosomal PD-L1 contributes to immunosuppression and is associated with anti-PD-1 response. *Nature*, *560*, 382–386.

Cheng, L., & Hill, A. F. (2022). Therapeutically harnessing extracellular vesicles. *Nature Reviews Drug Discovery*, *21*, 379–399.

Corso, G., Heusermann, W., Trojer, D., Görgens, A., Steib, E., Voshol, J., Graff, A., Genoud, C., Lee, Y., Hean, J., Nordin, J. Z., Wiklander, O. P. B., El Andaloussi, S., & Meisner-Kober, N. (2019). Systematic characterization of extracellular vesicle sorting domains and quantification at the single molecule—single vesicle level by fluorescence correlation spectroscopy and single particle imaging. *Journal of Extracellular Vesicles*, *8*, 1663043.

Del Prete, A., Salvi, V., Soriani, A., Laffranchi, M., Sozio, F., Bosisio, D., & Sozzani, S. (2023). Dendritic cell subsets in cancer immunity and tumor antigen sensing. *Cellular & Molecular Immunology*, *20*, 432–447.

Dooley, K., McConnell, R. E., Xu, K., Lewis, N. D., Haupt, S., Youniss, M. R., Martin, S., Sia, C. L., McCoy, C., Moniz, R. J., Burenkova, O., Sanchez-Salazar, J., Jang, S. C., Choi, B., Harrison, R. A., Houde, D., Burzyn, D., Leng, C., Kirwin, K., … Williams, D. E. (2021). A versatile platform for generating engineered extracellular vesicles with defined therapeutic properties. *Molecular Therapy*, *29*(5), 1729–1743.

Ghasemi, R., Lazear, E., Wang, X., Arefanian, S., Zheleznyak, A., Carreno, B. M., Higashikubo, R., Gelman, A. E., Kreisel, D., Fremont, D. H., & Krupnick, A. S. (2016). Selective targeting of IL-2 to NKG2D bearing cells for improved immunotherapy. *Nature Communications*, *7*, 12878.

Hansen, T. H., Connolly, J. M., Gould, K. G., & Fremont, D. H. (2010). Basic and translational applications of engineered MHC class I proteins. *Trends in Immunology*, *31*, 363–369.

Hickey, J. W., Vicente, F. P., Howard, G. P., Mao, H.-Q., & Schneck, J. P. (2017). Biologically inspired design of nanoparticle artificial antigen-presenting cells for immunomodulation. *Nano Letters*, *17*, 7045–7054.

Hogquist, K. A., Jameson, S. C., Heath, W. R., Howard, J. L., Bevan, M. J., & Carbone, F. R. (1994). T cell receptor antagonist peptides induce positive selection. *Cell*, *76*, 17–27.

Holohan, C., Van Schaeybroeck, S., Longley, D. B., & Johnston, P. G. (2013). Cancer drug resistance: An evolving paradigm. *Nature Reviews Cancer*, *13*, 714–726.

Jenkins, M. K., & Moon, J. J. (2012). The role of naive T cell precursor frequency and recruitment in dictating immune response magnitude. *Journal of Immunology*, *188*, 4135–4140.

Kobayashi, H., Shiba, T., Yoshida, T., Bolidong, D., Kato, K., Sato, Y., Mochizuki, M., Seto, T., Kawashiri, S., & Hanayama, R. (2024). Precise analysis of single small extracellular vesicles using flow cytometry. *Scientific Reports*, *14*, 7465.

Krieg, C., Létourneau, S., Pantaleo, G., & Boyman, O. (2010). Improved IL-2 immunotherapy by selective stimulation of IL-2 receptors on lymphocytes and endothelial cells. *Proceedings of the National Academy of Sciences of the United States of America*, *107*, 11906–11911.

Létourneau, S., van Leeuwen, E. M. M., Krieg, C., Martin, C., Pantaleo, G., Sprent, J., Surh, C. D., & Boyman, O. (2010). IL-2/anti-IL-2 antibody complexes show strong biological activity by avoiding interaction with IL-2 receptor alpha subunit CD25. *Proceedings of the National Academy of Sciences of the United States of America*, *107*, 2171–2176.

Levin, A. M., Bates, D. L., Ring, A. M., Krieg, C., Lin, J. T., Su, L., Moraga, I., Raeber, M. E., Bowman, G. R., Novick, P., Pande, V. S., Fathman, C. G., Boyman, O., & Garcia, K. C. (2012). Exploiting a natural conformational switch to engineer an interleukin-2 "superkine". *Nature*, *484*, 529–533.

Li, J., Li, J., Peng, Y., Du, Y., Yang, Z., & Qi, X. (2023). Dendritic cell derived exosomes loaded neoantigens for personalized cancer immunotherapies. *Journal of Controlled Release*, *353*, 423–433.

Liu, C., Liu, X., Xiang, X., Pang, X., Chen, S., Zhang, Y., Ren, E., Zhang, L., Liu, X., Lv, P., Wang, X., Luo, W., Xia, N., Chen, X., & Liu, G. (2022). A nanovaccine for antigen self-presentation and immunosuppression reversal as a personalized cancer immunotherapy strategy. *Nature Nanotechnology*, *17*(5), 531–540.

Lu, Z., Zuo, B., Jing, R., Gao, X., Rao, Q., Liu, Z., Qi, H., Guo, H., & Yin, H. (2017). Dendritic cell-derived exosomes elicit tumor regression in autochthonous hepatocellular carcinoma mouse models. *Journal of Hepatology*, *67*, 739–748.

Pitt, J. M., André, F., Amigorena, S., Soria, J.-C., Eggermont, A., Kroemer, G., & Zitvogel, L. (2016). Dendritic cell-derived exosomes for cancer therapy. *Journal of Clinical Investigation*, *126*, 1224–1232.

Poggio, M., Hu, T., Pai, C.-C., Chu, B., Belair, C. D., Chang, A., Montabana, E., Lang, U. E., Fu, Q., Fong, L., & Blelloch, R. (2019). Suppression of exosomal PD-L1 induces systemic anti-tumor immunity and memory. *Cell*, *177*, 414–427.e13.

Ren, J., Chu, A. E., Jude, K. M., Picton, L. K., Kare, A. J., Su, L., Montano Romero, A., Huang, P.-S., & Garcia, K. C. (2022). Interleukin-2 superkines by computational design. *Proceedings of the National Academy of Sciences of the United States of America*, *119*, e2117401119.

Robbins, P. D., & Morelli, A. E. (2014). Regulation of immune responses by extracellular vesicles. *Nature Reviews Immunology*, *14*, 195–208.

Robbins, P. F., Li, Y. F., El-Gamil, M., Zhao, Y., Wargo, J. A., Zheng, Z., Xu, H., Morgan, R. A., Feldman, S. A., Johnson, L. A., Bennett, A. D., Dunn, S. M., Mahon, T. M., Jakobsen, B. K., & Rosenberg, S. A. (2008). Single and dual amino acid substitutions in TCR CDRs can enhance antigen-specific T cell functions. *Journal of Immunology*, *180*(9), 6116–6131.

Rosenberg, S. A., Lotze, M. T., Yang, J. C., Topalian, S. L., Chang, A. E., Schwartzentruber, D. J., Aebersold, P., Leitman, S., Linehan, W. M., & Seipp, C. A. (1993). Prospective randomized trial of high-dose interleukin-2 alone or in conjunction with lymphokine-activated killer cells for the treatment of patients with advanced cancer. *JNCI: Journal of the National Cancer Institute*, *85*, 622–632.

Segura, E., Nicco, C., Lombard, B., Véron, P., Raposo, G., Batteux, F., Amigorena, S., & Théry, C. (2005). ICAM-1 on exosomes from mature dendritic cells is critical for efficient naive T-cell priming. *Blood*, *106*, 216–223.

Sellars, M. C., Wu, C. J., & Fritsch, E. F. (2022). Cancer vaccines: Building a bridge over troubled waters. *Cell*, *185*, 2770–2788.

Shi, X., Cheng, Q., Hou, T., Han, M., Smbatyan, G., Lang, J. E., Epstein, A. L., Lenz, H.-J., & Zhang, Y. (2020). Genetically engineered cell-derived nanoparticles for targeted breast cancer immunotherapy. *Molecular Therapy*, *28*, 536–547.

Silva, D.-A., Yu, S., Ulge, U. Y., Spangler, J. B., Jude, K. M., Labão-Almeida, C., Ali, L. R., Quijano-Rubio, A., Ruterbusch, M., Leung, I., Biary, T., Crowley, S. J., Marcos, E., Walkey, C. D., Weitzner, B. D., Pardo-Avila, F., Castellanos, J., Carter, L., Stewart, L., … Baker, D. (2019). De novo design of potent and selective mimics of IL-2 and IL-15. *Nature*, *565*(7738), 186–191.

Sockolosky, J. T., Trotta, E., Parisi, G., Picton, L., Su, L. L., Le, A. C., Chhabra, A., Silveria, S. L., George, B. M., King, I. C., Tiffany, M. R., Jude, K., Sibener, L. V., Baker, D., Shizuru, J. A., Ribas, A., Bluestone, J. A., & Garcia, K. C. (2018). Selective targeting of engineered T cells using orthogonal IL-2 cytokine-receptor complexes. *Science*, *359*, 1037–1042.

Stickney, Z., Losacco, J., McDevitt, S., Zhang, Z., & Lu, B. (2016). Development of exosome surface display technology in living human cells. *Biochemical and Biophysical Research Communications*, *472*, 53–59.

Théry, C., Duban, L., Segura, E., Véron, P., Lantz, O., & Amigorena, S. (2002). Indirect activation of naïve $CD4^+$ T cells by dendritic cell-derived exosomes. *Nature Immunology*, *3*, 1156–1162.

Théry, C., Witwer, K. W., Aikawa, E., Alcaraz, M. J., Anderson, J. D., Andriantsitohaina, R., Antoniou, A., Arab, T., Archer, F., Atkin-Smith, G. K., Ayre, D. C., Bach, J. M., Bachurski, D., Baharvand, H., Balaj, L., Baldacchino, S., Bauer, N. N., Baxter, A. A., Bebawy, M., … Zuba-Surma, E. K. (2018). Minimal information for studies of extracellular vesicles 2018 (MISEV2018): A position statement of the International Society for Extracellular Vesicles and update of the MISEV2014 guidelines. *Journal of Extracellular Vesicles*, *7*(1), 1535750.

Vandenborre, K., Van Gool, S. W., Kasran, A., Ceuppens, J. L., Boogaerts, M. A., & Vandenberghe, P. (1999). Interaction of CTLA-4 (CD152) with CD80 or CD86 inhibits human T-cell activation. *Immunology*, *98*, 413–421.

van Niel, G., D'Angelo, G., & Raposo, G. (2018). Shedding light on the cell biology of extracellular vesicles. *Nature Reviews Molecular Cell Biology*, *19*, 213–228.

Warashina, S., Zouda, M., Mohri, K., Wada, Y., Maeda, K., Watanabe, Y., & Mukai, H. (2022). $^{64}$Cu-labeling of small extracellular vesicle surfaces via a cross-bridged macrocyclic chelator for pharmacokinetic study by positron emission tomography imaging. *International Journal of Pharmaceutics*, *624*, 121968.

Yang, J. C., Sherry, R. M., Steinberg, S. M., Topalian, S. L., Schwartzentruber, D. J., Hwu, P., Seipp, C. A., Rogers-Freezer, L., Morton, K. E., White, D. E., Liewehr, D. J., Merino, M. J., & Rosenberg, S. A. (2003). Randomized study of high-dose and low-dose interleukin-2 in patients with metastatic renal cancer. *Journal of Clinical Oncology*, *21*(16), 3127–3132.

Yurtsever, A., Yoshida, T., Behjat, A. B., Araki, Y., Hanayama, R., & Fukuma, T. (2021). Structural and mechanical characteristics of exosomes from osteosarcoma cells explored by 3D-atomic force microscopy. *Nanoscale*, *13*, 6661–6677.

Zitvogel, L., Regnault, A., Lozier, A., Wolfers, J., Flament, C., Tenza, D., Ricciardi-Castagnoli, P., Raposo, G., & Amigorena, S. (1998). Eradication of established murine tumors using a novel cell-free vaccine: Dendritic cell-derived exosomes. *Nature Medicine*, *4*, 594–600.

## SUPPORTING INFORMATION

Additional supporting information can be found online in the Supporting Information section at the end of this article.

**How to cite this article:** Lyu, X., Yamano, T., Nagamori, K., Imai, S., Van Le, T., Bolidong, D., Ueda, M., Warashina, S., Mukai, H., Hayashi, S., Matoba, K., Nishino, T., & Hanayama, R. (2025). Direct delivery of immune modulators to tumour-infiltrating lymphocytes using engineered extracellular vesicles. *Journal of Extracellular Vesicles*, *14*, e70035. https://doi.org/10.1002/jev2.70035